NASA TECHNICAL NOTE NASA TN D-1857

NASA TN D-1857

LARGE-SCALE WIND-TUNNEL TESTS OF DESCENT PERFORMANCE OF AN AIRPLANE MODEL WITH A TILT WING AND DIFFERENTIAL PROPELLER THRUST

by Wallace H. Deckert, V. Robert Page, and Stanley O. Dickinson

Ames Research Center
Moffett Field, Calif.

NATIONAL AERONAUTICS AND SPACE ADMINISTRATION • WASHINGTON, D. C. • OCTOBER 1964

LARGE-SCALE WIND-TUNNEL TESTS OF DESCENT PERFORMANCE OF AN AIRPLANE MODEL WITH A TILT WING AND DIFFERENTIAL PROPELLER THRUST

By Wallace H. Deckert, V. Robert Page,
and Stanley O. Dickinson

Ames Research Center
Moffett Field, Calif.

NATIONAL AERONAUTICS AND SPACE ADMINISTRATION

For sale by the Office of Technical Services, Department of Commerce,
Washington, D.C. 20230 -- Price $1.00

LARGE-SCALE WIND-TUNNEL TESTS OF DESCENT PERFORMANCE OF AN AIRPLANE MODEL WITH A TILT WING AND DIFFERENTIAL PROPELLER THRUST

By Wallace H. Deckert, V. Robert Page,
and Stanley O. Dickinson

Ames Research Center
Moffett Field, Calif.

SUMMARY

Tests were conducted to determine the wing stall, performance, and longitudinal stability and control characteristics of a large model of a V/STOL tilt-wing transport aircraft. The scope of the tests was limited primarily to the low-speed transitional regime.

Test configurations included wing tilt angles from 0° to 40°, double-slotted trailing-edge flaps deflected from 0° to 60°, various wing leading-edge devices, such as partial-span and full-span Krüger flaps and slats, and several ramps that extended from the top of the fuselage to the tilted wing center section.

Test results show that air-flow separation over the tilted wing center section limited maximum lift and produced horizontal-tail buffet, that theoretical wing stall boundaries were optimistic, that low-speed descent angles were less than 5° for the various flap, slat, and ramp configurations tested, and that descent angles greater than 10° were obtained by operating the inboard propellers at a higher thrust level than the outboard propellers.

Pitch control with the variable incidence horizontal stabilizer was sufficient for trimmed 1 g level flight throughout the transition range tested to a minimum airspeed of 40 knots. An additional pitch control device, such as a tail rotor, would be required for maneuvering and steady climbing flight, including the landing wave-off condition for a configuration with no wing tilt.

The tail on and off longitudinal static stability was slightly unstable throughout the transitional flight regime tested.

INTRODUCTION

NASA investigations of the aerodynamic characteristics of propeller-driven tilt-wing aircraft have included wind-tunnel and flight tests. The results of the wind-tunnel tests of the first large-scale, four-propeller,

tilt-wing model (refs. 1 and 2) are of particular interest for a background to this report. In references 1 and 2 it was indicated that air-flow separation on tilt-wing aircraft would limit descent performance and cause buffeting in the low-speed transitional flight regime. Flight tests of the VZ-2 tilt-wing airplane (ref. 3) also indicated that the most critical region of operation of the VZ-2 was during decelerating conversion and/or descent where the effects of air-flow separation and wing stall led to buffeting, erratic motions, and general deficiencies in handling qualities. For the model of references 1 and 2, premature air-flow separation occurred from the tilted wing center section outside the propeller slipstream and from an outboard area of the wing between the nacelles which was only partially immersed in the propeller slipstream.

The objectives of the wind-tunnel investigation of this report were (1) to determine whether the problems revealed in references 1 and 2 were present on a model which closely resembled a V/STOL tilt-wing transport aircraft, (2) to determine the effects of various spanwise extents of leading-edge devices on the onset of air-flow separation, and (3) to determine descent performance with the inboard propellers operating at high thrust relative to the outboard propellers.

NOTATION

A total disk area of all four propellers, $4\pi r^2$, sq ft

b wing span, ft

c wing chord parallel to plane of symmetry, ft

$\bar{c}$ mean aerodynamic chord, $\frac{2}{S}\int_0^{b/2} c^2\,dy$, ft

C_D drag coefficient including thrust, $\frac{\text{measured drag}}{q_\infty S}$

C_L lift coefficient including thrust, $\frac{\text{measured lift}}{q_\infty S}$

C_{L_α} slope of lift curve, per deg

C_m pitching-moment coefficient, $\frac{\text{pitching moment}}{q_\infty S\bar{c}}$

C_{m_α} $\frac{\partial C_m}{\partial \alpha}$

$C_{m_{i_t}}$ $\frac{\partial C_m}{\partial i_t}$

D propeller diameter, ft

g acceleration of gravity, 32.2 ft/sec^2

i_t incidence of horizontal tail relative to fuselage reference line, deg

i_w incidence of wing root chord with respect to fuselage reference line with wing down, deg (0 for model of this report)

J propeller advance ratio, $\frac{V_\infty}{nD}$

L lift including thrust component, lb

n propeller rotational velocity, rps

q_∞ free-stream dynamic pressure, lb/sq ft

R Reynolds number, $\frac{\rho V_\infty \bar{c}}{\mu}$

r propeller blade radius, ft

S wing area, sq ft

T total thrust of all four propellers, lb

T_c' thrust coefficient, $\frac{T}{q_\infty S}$

V airspeed scaled for W/S = 70 lb/ft^2 airplane, knots

V_S descent rate, ft/min

V_∞ free-stream tunnel velocity, fps or as noted

W gross weight, lb

α angle of attack of fuselage reference line, deg

α_w geometric angle of attack of wing root chord, $\delta_w + \alpha + i_w$, deg

β propeller blade angle at 3/4 r, deg

γ descent angle, deg

δ_f flap deflection relative to local wing chord, deg

δ_w wing tilt angle of root chord relative to fuselage reference line, deg

μ coefficient of viscosity, slugs/ft-sec

ρ mass density of air, slugs/ft^3

Relationships of Coefficients Based on Free-Stream and Propeller Slipstream Dynamic Pressure

$$q_s = q_\infty + \frac{T}{A}$$

$$C_{T_S} = \frac{T}{q_s A} = \frac{T_c'}{T_c' + A/S} = \frac{T_c'}{T_c' + 1.38}$$

$$1 - C_{T_S} = \frac{q_\infty}{q_s}$$

$$C_{L_S} = C_L(1 - C_{T_S})$$

MODEL AND APPARATUS

The model installed in the center of the 40- by 80-foot test section is shown in figures 1 and 2. The model resembles very closely the XC-142 V/STOL airplane at 0.6 scale.

A three-view drawing of the model is shown in figure 3. Pertinent geometric characteristics (table I) of the wing were: span, 40.5 feet; aspect ratio, 8.4; taper ratio, 0.55; and mean aerodynamic chord, 4.99 feet. The wing airfoil section for the model (table II) was an NACA 23017 with the leading edge modified to the geometry of an NACA 63-318 section. (The airfoil section of the XC-142 airplane is an NACA 63-318 section.)

A typical section of the double-slotted trailing-edge flap is shown in figure 4; the coordinates are presented in table II. The large trailing-edge flap extended full span, except for nacelle cutouts, and was deflected a maximum of 60°.

Typical sections of the various wing leading-edge devices that were evaluated are shown in figure 5. The wing leading-edge configurations included partial-span and full-span extents of a 0.10c Krüger flap and 0.2c slats. The partial-span leading-edge devices extended from 43.7- to 60.7-percent and from 86.4- to 100-percent semispan.

The geometric characteristics of various ramps that extended from the top of the fuselage to the tilted wing center section are shown in figure 6. The basic short fore and aft ramps were installed for most of the runs. The modified fore and aft ramps were about twice the length of the basic fore and aft ramps, respectively.

The geometric characteristics of the three-bladed model propellers are shown in figure 7. The solid aluminum model propellers had a diameter of

9.3 feet, an activity factor, A.F., of 121 per blade, and rotation was such that the outboard blade of all four propellers rotated upward. Each propeller was shaft mounted on a gear box and driven by an electric motor. The four motors were operated in parallel from a variable-frequency power supply.

TEST AND PROCEDURE

Tests were made at free-stream tunnel velocities from 17 to 66 knots (q_∞ = 1 to 15, Reynolds number 0.9 to 3.6 million based on the wing mean aerodynamic chord of 4.99 ft). For each run the fuselage angle of attack was varied while the tunnel dynamic pressure, propeller speed, and propeller blade angle were held fixed.

The three-component longitudinal data presented in the figures include the propeller thrust components as well as the model aerodynamic components. The propeller thrust characteristics were determined by wind-tunnel tests at a thrust axis inclination of 0° with the propeller on and off the model. Figure 8 shows the relationship of the thrust coefficients T_c' and C_{T_s} for this model so that the coefficients based on free-stream dynamic pressure may be readily converted to coefficients based on propeller slipstream dynamic pressure as desired.

Pitching moments are presented about the center shown in figure 9. The moment center used for calculation was varied slightly with wing tilt angle in accordance with a center-of-gravity change due to wing mass effects expected for a tilt-wing transport aircraft. For a 0° wing tilt angle, the horizontal moment center was at 0.23 $\bar{c}$.

The model was mounted on faired struts in a manner which isolated the strut forces from the model. Tunnel wall corrections and strut-to-model interference factors were not applied to any of the data.

RESULTS

Figures 10 to 26 are the general results of configurations having partial-span Krüger flaps, full-span slats, and the combination of full-span slats with differential spanwise propeller thrust.

DISCUSSION

Aerodynamic Characteristics of the Basic Configuration

Three component longitudinal force and moment data, C_L, C_D, and C_m, are presented at several thrust coefficients in figures 10 and 11 for the basic configuration for wing tilt angles, δ_w, of 20° and 30° and flaps deflected

60°. The basic configuration consisted of partial-span Krüger flaps, the basic short fore and aft ramps over the wing center section (fig. 6), a blade angle setting, β of 10° on all four propellers, and a horizontal-tail setting of +20°.

At $T_c' > 0$, maximum lift was limited by air-flow separation from the portion of the tilted wing center section that was unprotected by the propeller slipstream and from an area on the wing between the inboard and outboard nacelles. As shown on figures 10 and 11, the air-flow separation limited the descent capability of the basic configuration to descent angles of about 2° or 3°. This air-flow separation originated on the upper surface of the wing just aft of the leading edge and at a spanwise location above the sides of the fuselage. As the fuselage angle of attack was increased, the separated area progressed aft to the wing root trailing edge and outboard into the area immersed in the inboard propeller slipstream and along the upper surface of the fuselage to the empennage. At the higher fuselage angles of attack, the stalled center section wake enveloped about two-thirds of the vertical tail.

The air-flow separation at the wing center section was generally associated with buffeting of the horizontal tail. Typical buffet intensities, measured at the tip of the horizontal tail, are shown in figure 12 for the basic configuration with a wing tilt angle of 20°. Figure 12 shows that the buffeting level increased rapidly as the fuselage angle of attack was increased above 4°. Thus the test result (figs. 10 to 12) supported the general conclusions of references 1 and 2 that the flight envelope of a tilt-wing aircraft with an exposed wing center section may be limited by separation over the wing center section.

Incremental flap lift and drag coefficients are presented in figure 13 for the 0° untilted wing configuration. At constant thrust, the flap lift coefficient increased approximately linearly from 0° to 60° flap deflection. The flap drag coefficient remained unchanged from 0° to about 30° flap deflection and increased rapidly from 30° to 60° deflection. Figure 13 indicates that both lift and drag would increase if the flaps were deflected beyond 60°. Hence, flap deflections greater than 60° may be desirable for higher descent angles during STOL type landings. Vane and flap surface tuft observations and surface pressure data, corresponding to test conditions of figure 13, indicated that the flow over the surface of all the vanes and inboard flap was attached but the flow over the outboard flaps was separated. The area of attached flow over the flaps progressively moved outboard as the wing tilt angle was increased. For a wing tilt of 40° and flap deflection of 60° and T_c' values 3.5 to 7.4 the air flow was attached near the surface of all the vanes and flap except the flap segment outboard of the outboard nacelle. (Masted tufts a few inches above the flap surfaces indicated "separated" flow even when surface tufts indicated attached flow.)

Effect of Wing Leading-Edge Devices

Several high-lift devices were tested in various partial- and full-span configurations on the wing leading edge. Air-flow separation from the outboard portion of the wing between the nacelles was delayed when the partial-span Krüger flaps were replaced with partial-span slats. The onset of air-flow separation over the outboard portion of the wing and the wing root was further delayed when the spanwise extent of the slats was increased to cover the exposed wing leading edge from the fuselage to the wing tip.

Longitudinal characteristics for the full-span slat configuration are presented in figures 14 and 15 for wing tilt angles of 20° and 30° and flap deflections of 60°. Descent angles, based on $C_{L_{max}}$, of 4° to 6° were obtained with the full-span slats. The angle of attack at which air-flow separation occurred outboard on the wing was significantly increased (no such separation occurred for any of the test points shown in fig. 14 or 15 at $T_c' > 0$). However, this large delay in separation was not reflected in the descent performance, based on $C_{L_{max}}$, because the separation at the wing center section largely determined the angle of attack for maximum lift. The buffeting characteristics of the horizontal tail remained about the same as those of the basic configuration.

Several wing center section configurations were tested to determine the extent to which the air-flow separation could be delayed or contained. The configurations included various combinations of the basic short fore and aft ramps, modified fore and aft ramps about twice the length of the basic ramps, a slat replacing the fore ramp, and fences (extending from the front edge of the fore ramp to the aft edge of the aft ramp) on the wing above the sides of the fuselage. A comparison of the force data is presented in figure 16 for a configuration with the basic short fore and aft ramps and for a configuration with a long fore ramp with added side wrap-around fairings and a long aft ramp. None of the wing center section configurations tested significantly reduced the air-flow separation problem or changed the buffeting characteristics of the horizontal tail. Figure 16 shows that no improvement in force data was obtained.

For a tilt-wing aircraft with an exposed wing center section there appears to be little point in optimizing leading-edge devices for increased descent performance until separation has been eliminated from the wing center section.

Effect of Spanwise Distribution of Propeller Thrust

Tests were conducted to determine the effect of varying the wing spanwise lift and drag distribution by operating the inboard and outboard propellers at different thrust settings. For each run, the inboard and outboard propeller speeds were equal and held constant with the inboard propeller blade angle higher than the outboard. The propeller thrust was controlled by propeller blade pitch angle in an attempt to obtain higher downwash angles

in the slipstream due to the downward rotation of the propeller over the wing leading edges in the region of the fuselage where the effects of air-flow separation were predominant in determining maximum lift coefficient. The descent performance should then be improved in two ways: (1) by the higher drag at a given lift coefficient obtained by a distorted span loading and; (2) by the increase in the maximum values of lift coefficient before the onset of air-flow separation.

Several tests at various differential propeller blade angle settings are compared at the same average thrust coefficient in figure 17 for a 20° wing-tilt configuration. Both maximum lift and descent capability increased as differential propeller thrust was increased.

The largest differential propeller thrust settings tested were with an inboard and outboard propeller blade angle of 14° and 0°, respectively. Force data at several average thrust settings are shown in figures 18 and 19 for the β = 14/0 configuration with wing tilt angles of 20° and 30°, flaps deflected 60°, and full-span slats. It is seen that the descent capability was significantly increased to descent angles greater than 10°.

The individual propeller thrust coefficients shown in figures 18 and 19 are approximate values obtained from two thrust calibrations, one with differential blade angle settings of 14° and 0° and the other with all propellers set at 14° (see fig. 8). At a given advance ratio, the thrust of the inboard propeller set at β = 14 was therefore taken to be independent of the thrust setting on the outboard propeller. With this assumption the thrust of the outboard propeller with β = 0 varied from slightly negative to slightly positive for the range of average thrust coefficients shown on figures 18 and 19.

With full-span slats on the wing, and average thrust coefficients of 1.1 or more, the flow over the portion of the wing behind the outboard propeller did not separate until the geometric wing angle of attack was 40° or more. With the outboard propellers removed, the outboard portion of the wing separated at a wing geometric angle of attack of 28° (T_C' = 2.6) and as shown on figure 17, the two-propeller configuration had essentially no descent capability. Why an outboard propeller producing little positive thrust, if any, protects the wing much more than no outboard propeller is of interest and worthy of future investigations. A strip analysis of the propeller set at β = 0, for the conditions of figure 17, showed that approximately the inboard half radius of the highly twisted blades was producing positive thrust although the integrated propeller thrust was slightly negative. Since the tip of the outboard propeller overlapped the inboard propeller and extended beyond the wing tip, a significant positive propeller slipstream component probably existed over most of the outboard portion of the wing even if the outboard propeller was producing a little negative total thrust.

The differential propeller thrust operation affected the span loading so that the drag at a given lift coefficient was greater, and it also delayed the onset of wing center section air-flow separation. With the wing tilted

20°, aft fuselage air-flow separation was delayed for about 6° to 7° fuselage angle of attack, which was a greater improvement than that realized from any of the modified ramp, slat, or fence combinations tested. The decrease in the horizontal-tail buffet intensities as a result of delaying the wing center section air-flow separation is shown in figure 12.

Summary force data comparing the differential propeller thrust configuration to the partial-span Krüger flap and full-span slat configurations previously discussed are shown in figure 20.

Descent Performance

Descent performance is summarized in figure 21. For the subject tilt-wing model, descent performance depends upon what one considers the limiting condition to be, that is, wing center section air-flow separation, aft fuselage air-flow separation, wing root air-flow separation, a particular horizontal-tail buffet intensity, $C_{L_{max}}$, the angle of attack at which air-flow separation occurs on the outboard portion of the wing, and so forth.

If the first appearance of wing center section air-flow separation were selected as the criteria, it could be shown that the subject model in any configuration tested would not be capable of 1 g level flight throughout the transition range. This would probably be a pessimistic interpretation of the tests. Figure 21 is based on the angle of attack at which wing air-flow separation occurred outboard of the inboard nacelle, which in many cases was beyond the angle of attack for $C_{L_{max}}$. This presentation is optimistic because no flight margin is included, the fuselage angle of attack is not restricted, and the other possible limitations previously mentioned are ignored. Thus figure 21 represents a maximum possible descent performance boundary. The degree of optimism of figure 21 can only be determined by flight testing the configuration.

Figure 21 shows that for the basic configuration (partial-span Krüger flaps and trailing-edge flaps deflected 60°) the descent capability is 5° or less at airspeeds below 60 knots. Descent performance, based on outboard wing air-flow separation, was significantly increased by incorporating full-span slats and by the use of differential propeller thrust. With the wing tilted 30° and for an airspeed of 50 knots, rate of descent was about 200, 700, and 1200 ft/min, respectively, for the configurations with partial-span Krüger flaps, full-span slats, and full-span slats with differential propeller thrust.

Longitudinal Stability and Control

Figure 22 presents the longitudinal static stability (C_{m_α}) at various thrust coefficients and wing tilt angles for the basic configuration with and without a tail and with the fuselage at 0° angle of attack. With the tail off

and no wing tilt, C_{m_α} was slightly positive (unstable) and became more unstable as either wing tilt angle or thrust coefficient increased. With or without the tail the stability characteristics were similar, but without the tail, the C_{m_α} was more unstable. At higher fuselage angles of attack, tail on or off, C_{m_α} values were similar to those of figure 22 or somewhat more unstable.

The effectiveness of the horizontal tail is presented in figure 23 for wing tilt angles of 0°, 20°, and 40° and flaps deflected 60°.

Figure 23 shows that the pitching moment was nearly trimmed with the wing tilted 20°, a T_c' of 2.0, and the incidence of the horizontal tail set at 0°. This point corresponds to a shallow descent at an airspeed of 60 knots (W/S = 70). It is also seen that pitch control with only tail incidence was not sufficient to trim the 20° wing tilt configuration for a T_c' of 3.5, which corresponds to shallow climbing flight at about 55 knots airspeed. These results are typical throughout the transition range tested; that is the model could be trimmed with only tail incidence for 1 g level flight for wing tilt angles from 0° to 40° at the low forward speeds, but an additional pitch control device, such as a tail rotor, would be required for climbing flight.

The largest measured value of $C_{m_{i_t}}$ was 0.065 per degree, obtained with the wing untilted and the propellers operating at differential thrust settings such that the inboard propeller T_c' was about 5.0. Values of $C_{m_{i_t}}$ of 0.039 to 0.040 were obtained with the wing tilted 20° to 40°. This variation in $C_{m_{i_t}}$ was probably caused by variations in the q_t/q_∞ ratio as described in the following paragraphs.

The fuselage angle-of-attack range for which the inboard propeller slipstream significantly increased the velocity over the tip of the horizontal tail is shown in figure 24 for the wing at 0° tilt angle and the trailing-edge flaps deflected 60°. The outboard q_t/q_∞, measured near the tip of the horizontal tail, reached a maximum of 4.3 at $\alpha = +8^\circ$. The inboard q_t/q_∞, measured at a spanwise location above the side of the fuselage, was approximately 0.7 throughout the angle-of-attack range.

For wing tilt angles of 20° and 30° and flap deflections of 60°, the outboard q_t/q_∞ rapidly increased and/or decreased as α was increased, depending on the thrust setting and separation characteristics over the wing center sections and outboard portions of the wing (fig. 25). Inboard q_t/q_∞ values of 0 were obtained for wing tilt angles of 20° or 30° at the higher fuselage angles of attack as typically shown by figure 25.

The horizontal-tail buffeting was a function of the air-flow separation over the wing center section and the effect of the inboard propeller slipstream on the local velocity over the tip of the horizontal tail. Some buffet occurred either whenever the wake from the separated center section enveloped the tail or whenever the outboard q_t/q_∞ ratio was much greater than the inboard q_t/q_∞ due to slipstream effects.

Comparison of Theoretical and Experimental Wing Stall Boundaries

A comparison of theoretical and experimental wing angle of attack for $C_{L_{max}}$ and the wing angle of attack for the onset of wing air-flow separation outboard of the inboard nacelle is shown in figure 26. The comparison is presented as a function of $(T/A)/q_\infty$ which is directly related to the ratio of slipstream to free-stream velocity. The theory (ref. 4) is a frequently used one in which the free-stream and propeller component velocities are vectorially added for estimated wing stall boundaries for tilt-wing VTOL aircraft. The theoretical assumptions are that (1) the slipstream component of an inclined propeller can be computed from simple momentum theory, (2) the wing is fully immersed in a fully developed slipstream, and (3) rotational effects of the slipstreams are small.

At $(T/A)/q_\infty$ of 4, experimental $C_{L_{max}}$ occurred at about 35° wing angle of attack compared to a predicted value of 65° angle of attack. One of the reasons for the lack of correlation is that $C_{L_{max}}$ was limited by air-flow separation at the wing center section instead of directly behind the propellers. It is apparent that predicted descent performance of a tilt-wing aircraft may not be realistic if areas that are not immersed in the propeller slipstreams are ignored. Adjusting the theory to account for only the specific area outside the propeller slipstreams may also yield optimistic estimates since air-flow separation which originates in the unprotected area may progress into significant portions of the immersed area.

The theoretical boundary for the onset of wing air-flow separation was also optimistic for this model when the area of interest was limited to the portion of the wing outboard of the inboard nacelle which was immersed in the propeller slipstream. Air-flow separation originated in this outboard wing area, instead of being the result of spreading from an unprotected area into the immersed area. At a $(T/A)/q_\infty$ of 4, air-flow separation occurred between the nacelles at about 57° wing angle of attack compared to a predicted angle of attack of 80°. The theory may be empirically corrected to agree with the experimental angle of attack for outboard wing air-flow separation on this model if the propeller thrust is assumed to be about 0.6 of the actual thrust.

The above discussion applies to the typical operation in which all four propellers produce approximately equal thrust. As stated in the section on differential spanwise propeller thrust, separation over the outboard portion of the wing was delayed for an additional 12° angle of attack with the outboard propellers at approximately zero thrust compared to the results with the outboard propellers removed. Thus, for the same average conditions, local conditions signficantly influenced experimental wing stall boundaries.

CONCLUSIONS

Wind-tunnel tests of a large-scale tilt-wing model indicate that significant improvement can be made in the stall boundaries and descent performance in the low-speed transition speed range. For a wing tilt of 30° at 50 knots the descent performance was increased by 500 ft/min when full-span slats were used instead of partial-span Krüger flaps and an additional 500 ft/min increase in descent performance can be obtained by differential propeller thrust across the wing span.

Theoretical boundaries for air-flow separation or stall were grossly optimistic compared to the experimental results obtained for the model of this investigation.

Ames Research Center
National Aeronautics and Space Administration
Moffett Field, Calif., July 17, 1964

REFERENCES

1. Weiberg, James A., and Holzhauser, Curt A.: Large-Scale Wind-Tunnel Tests of an Airplane Model With an Unswept, Tilt Wing of Aspect Ratio 5.5, and With Four Propellers and Blowing Flaps. NASA TN D-1034, 1961.

2. Weiberg, James A., and Giulianetti, Demo J.: Large-Scale Wind-Tunnel Tests of an Airplane Model With an Unswept Tilt Wing of Aspect Ratio 5.5, and With Various Stall Control Devices. NASA TN D-2133, 1964.

3. Pegg, Robert J.: Summary of Flight-Test Results of the VZ-2 Tilt-Wing Aircraft. NASA TN D-989, 1962.

4. Cromwell, Charles H., III, and Payne, Henry E., III: A Stability Analysis of Tilt-Wing Aircraft (Analytical). Princeton University Rep. 477, 1960.

TABLE I.- GEOMETRIC DIMENSIONS OF THE MODEL

Dimension	Wing	Horizontal surface	Vertical surface
Area, sq ft	196.5	50.4	46.7
Span, ft	40.5	16.0	9.35
$\bar{c}$, ft	4.99	3.27	5.60
Aspect ratio	8.35	5.08	1.87
Taper ratio	.55	.50	.25
Geometric twist, deg	3.7° Washout	0	0
Dihedral from reference plane, deg	-2.12	0	0
Airfoil section	Modified NACA 23017	0015 Root 0012 Tip	0018 Root 0012 Tip
Sweep of leading edge, deg	6.67	14.7	32.7
Sweep of c/4, deg	4.7	11.0	25.7
Sweep of trailing edge, deg	-1.3	0	0
Root chord, ft	6.26	4.20	8.00
Tip chord, ft	3.44	2.10	2.00

TABLE II.- STREAMWISE COORDINATES OF WING, FLAP, AND VANE IN PERCENT OF WING CHORD

Wing[1]			Flap			Vane		
x	y_{upper}	y_{lower}	x	y_{upper}	y_{lower}	x	y_{upper}	y_{lower}
1.41	2.72	-2.00	0	-1.19	-1.19	0	0	0
2.82	3.78	-2.85	.8	.61	-2.63	.39	.96	-.96
4.23	4.60	-3.49	1.7	1.45	-2.89	.77	1.32	-1.20
5.64	5.29	-3.98	2.5	2.06	-2.95	1.15	1.59	-1.36
7.05	5.96	-4.37	3.3	2.58	-2.95	1.54	1.78	-1.45
10.58	7.32	-5.15	5.0	3.45	-2.78	2.31	2.16	-1.53
14.11	8.40	-5.64	6.6	4.05	-2.50	3.08	2.40	-1.46
17.64	9.22	-5.97	8.2	4.43	-2.17	3.85	2.60	-1.27
21.17	9.62	-6.24	9.9	4.50	-1.94	4.62	2.75	-.98
28.22	9.85	-6.70	11.5	4.35	-1.68	5.39	2.82	-.67
35.27	9.70	-6.89	13.2	4.01	-1.42	6.16	2.86	-.35
42.33	9.30	-6.70	14.85	3.68	-1.17	6.93	2.87	-.07
49.38	8.62	-6.35	16.50	3.33	-.96	7.70	2.86	.15
56.42	7.77	-5.86	18.15	3.02	-.77	8.46	2.80	.31
63.45	6.87	-5.25	19.80	2.67	-.60	9.24	2.69	.45
70.50	5.78	-4.47	23.10	2.01	-.31	10.77	2.33	.59
77.60	4.61	-3.56	26.40	1.35	-.08	12.32	1.79	.54
84.60	3.30	-2.57	29.70	.69	0	13.85	.99	.35
91.70	1.86	-1.52	31.40	.31	-.03	14.62	.52	.20
100.00	.17	-.17	33.0	.04	0	15.40	.07	0
L.E. radius = 2.12% c			L.E. radius = 0.56% c			L.E. radius = 0.21% c		

[1]23017 airfoil with modified leading edge

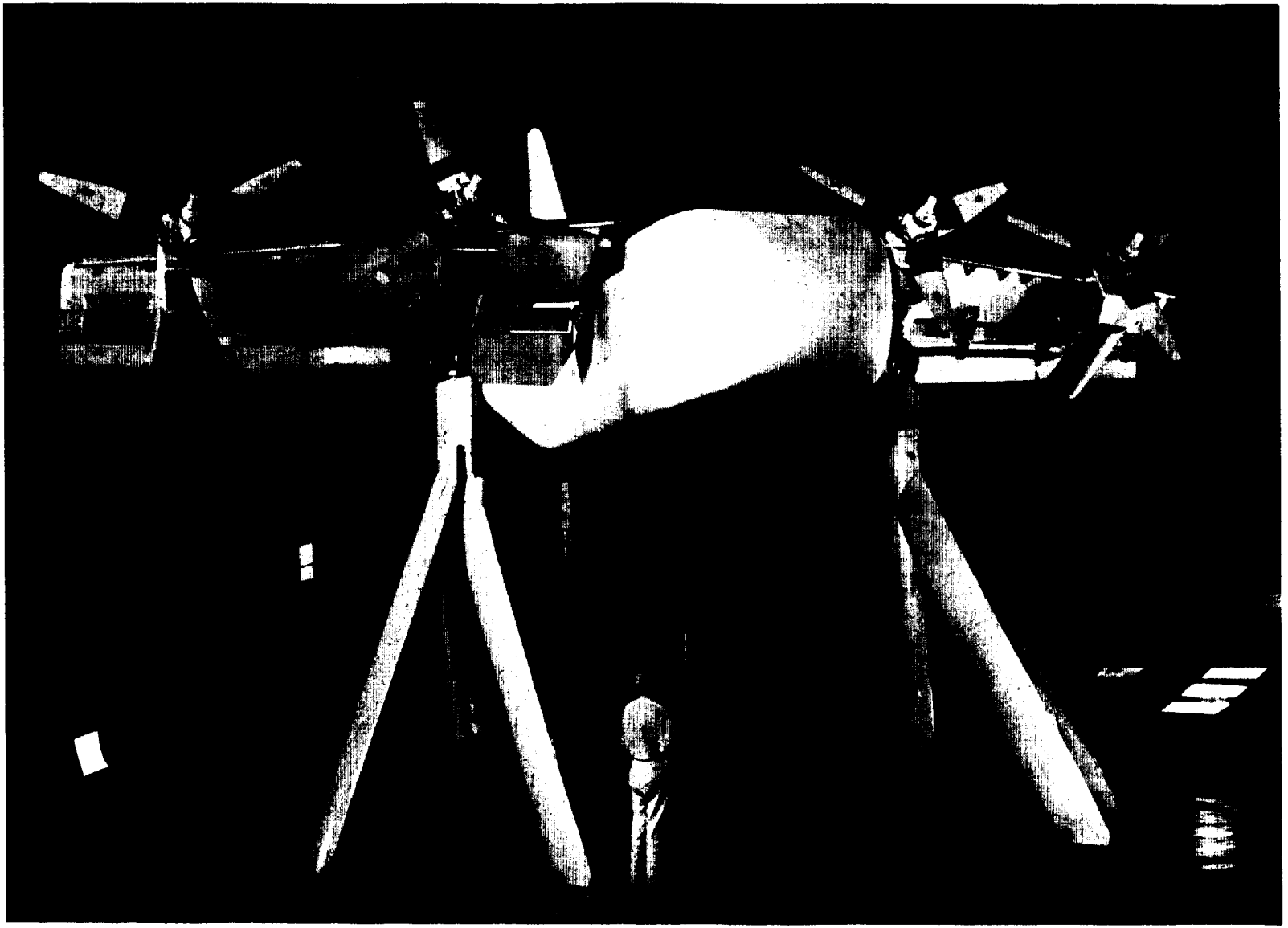

A-29909

Figure 1.- Photograph of the model in the Ames 40- by 80-foot wind tunnel.

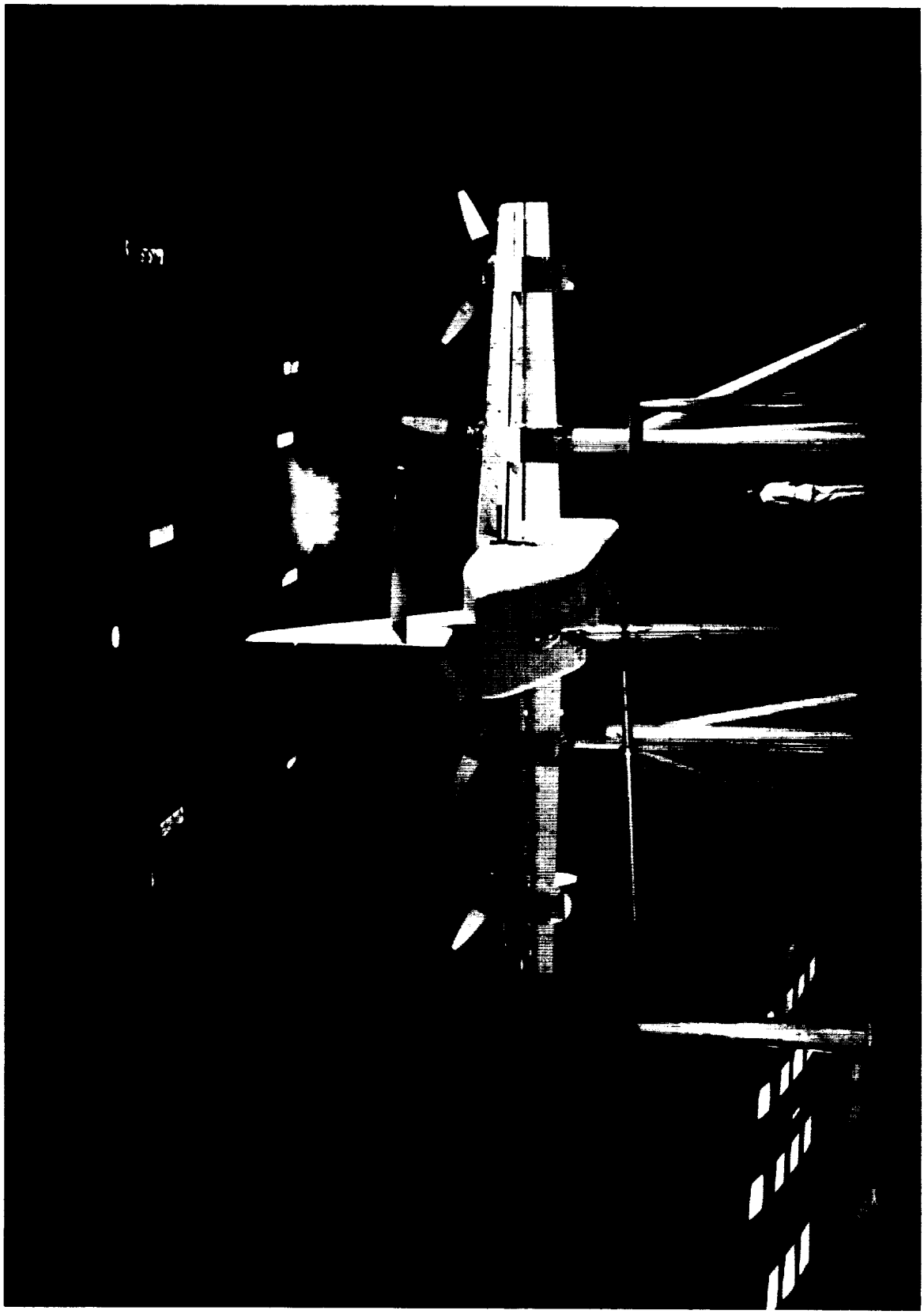

A-29910

Figure 2.- Rear view of the model.

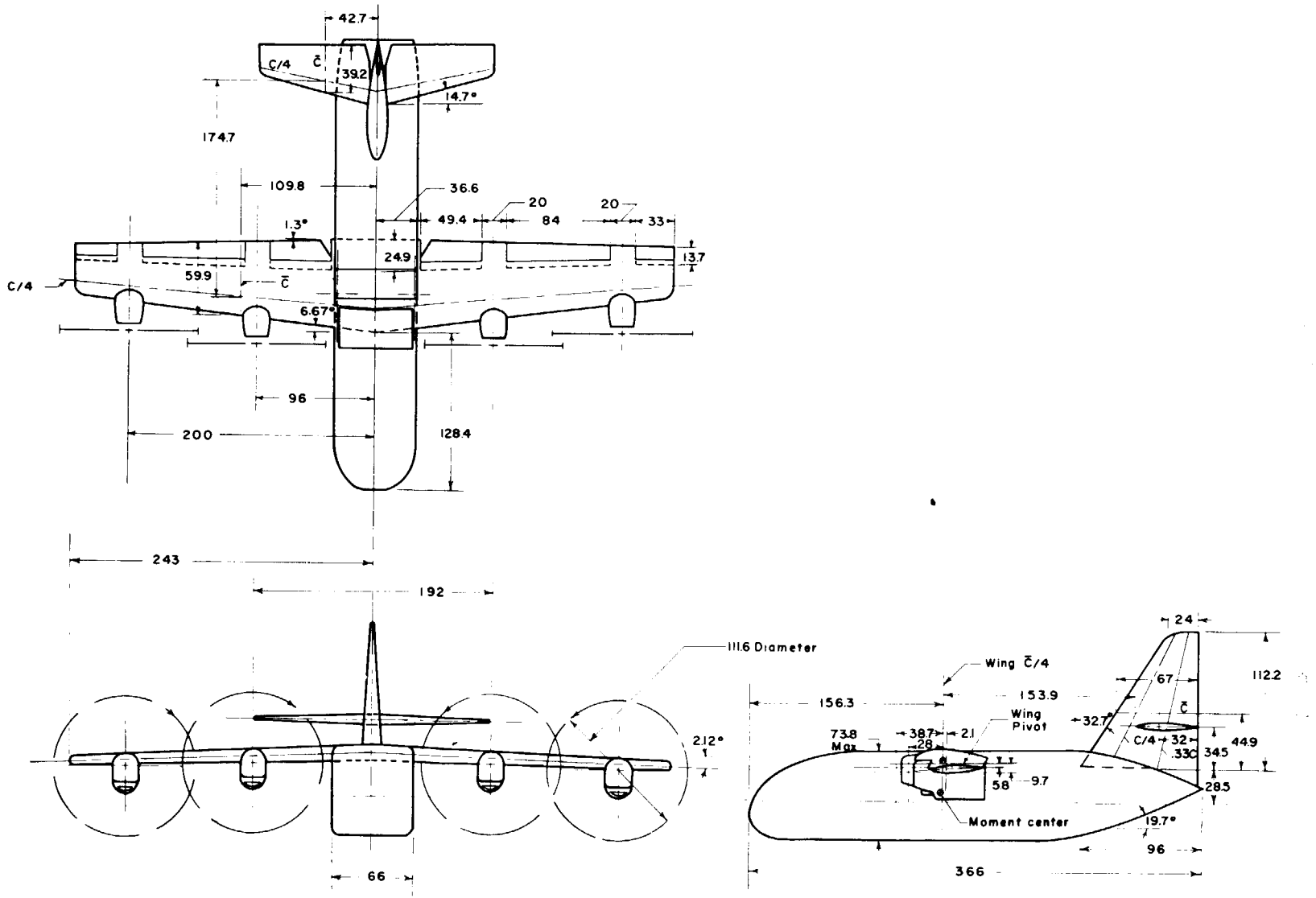

Figure 3.- Model 3 view (dimensions in inches except as noted).

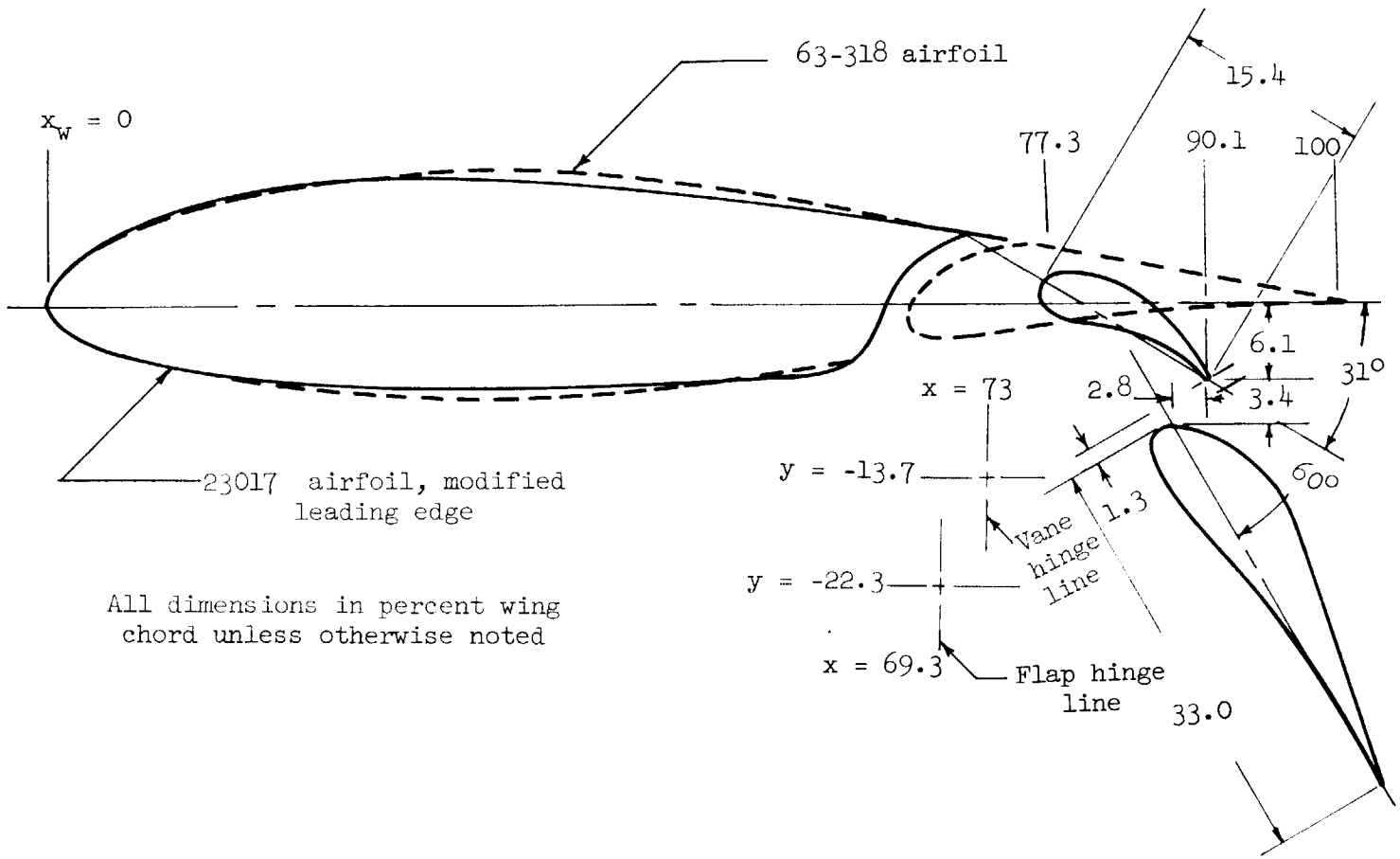

Figure 4.- Details of wing airfoil and trailing-edge flap.

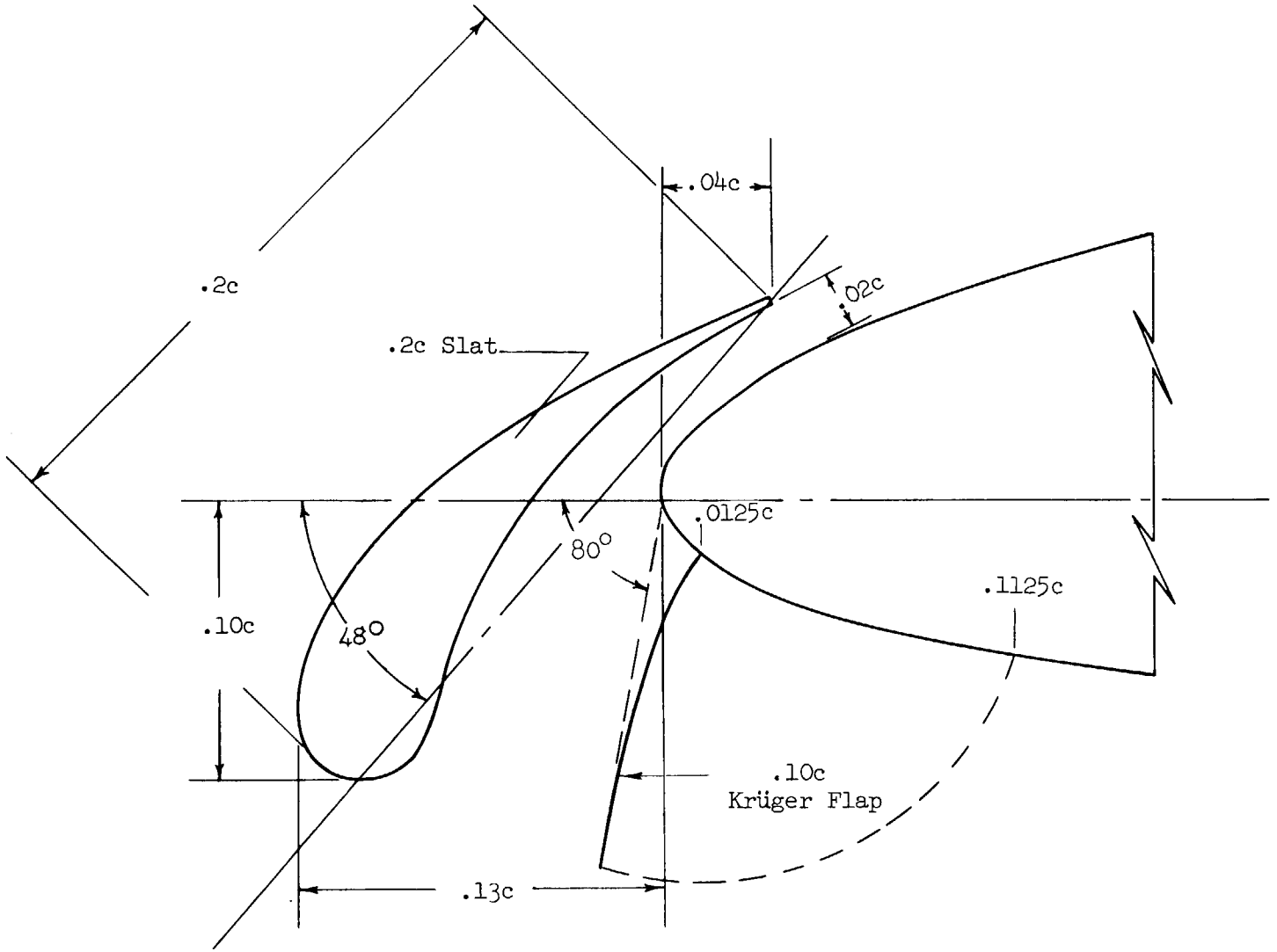

Figure 5.- Details of wing leading-edge devices.

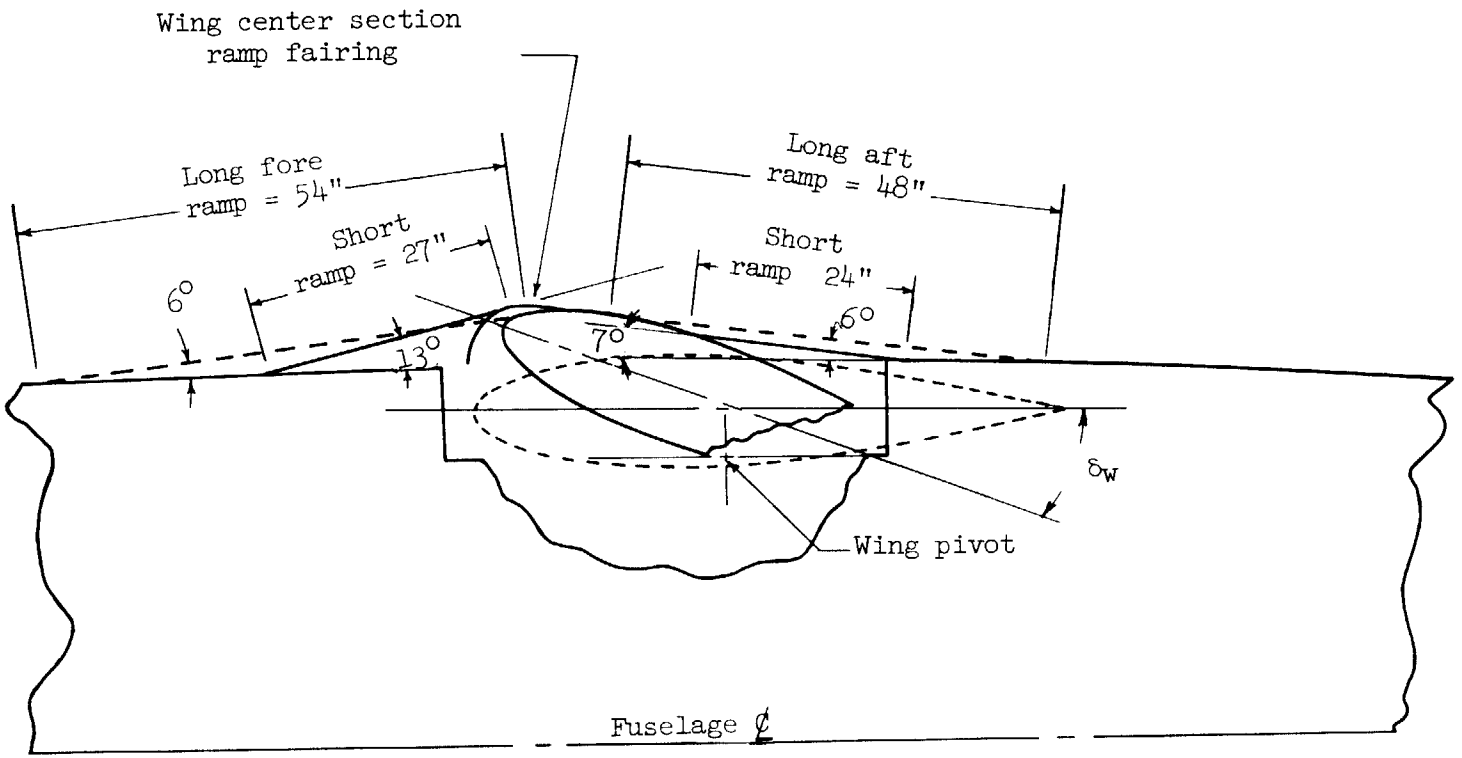

Figure 6.- Details of wing center-section ramp.

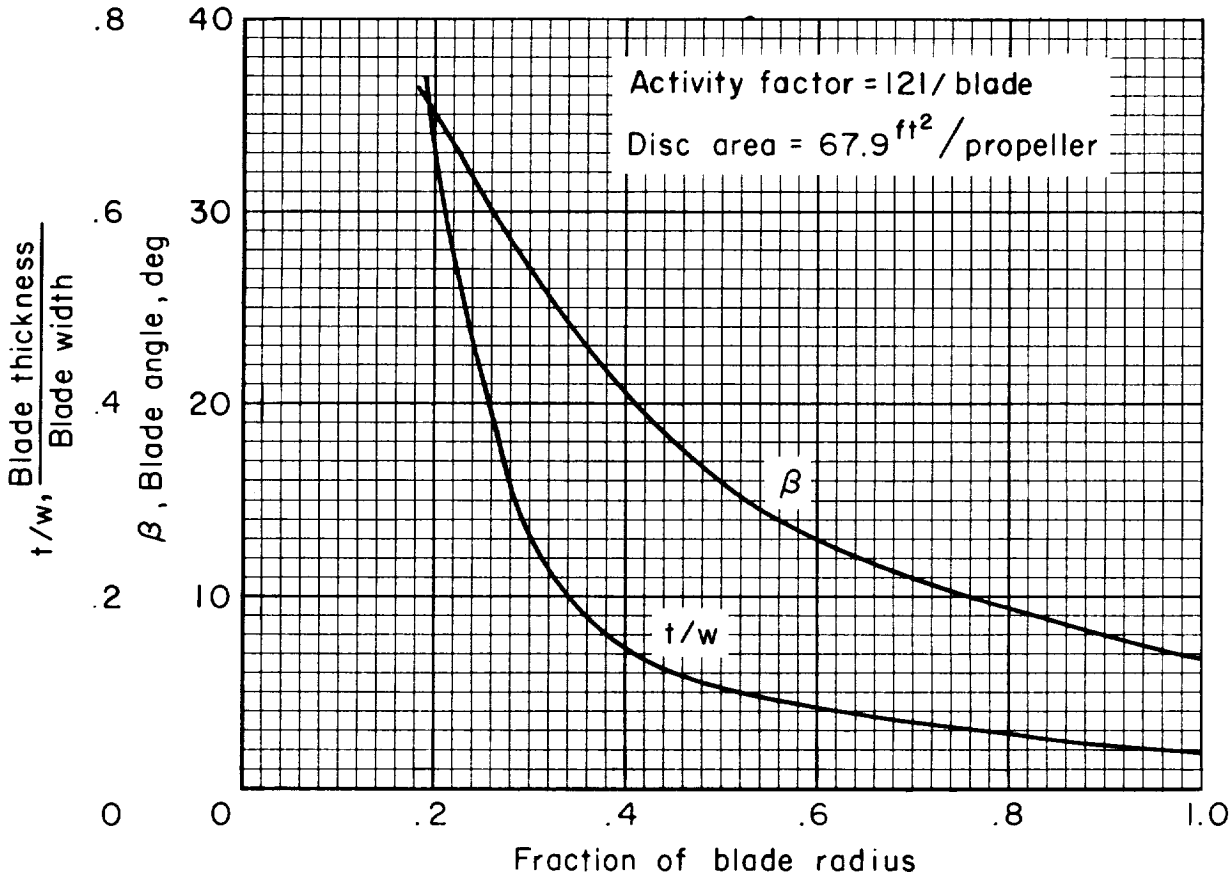

Figure 7.- Propeller blade characteristics.

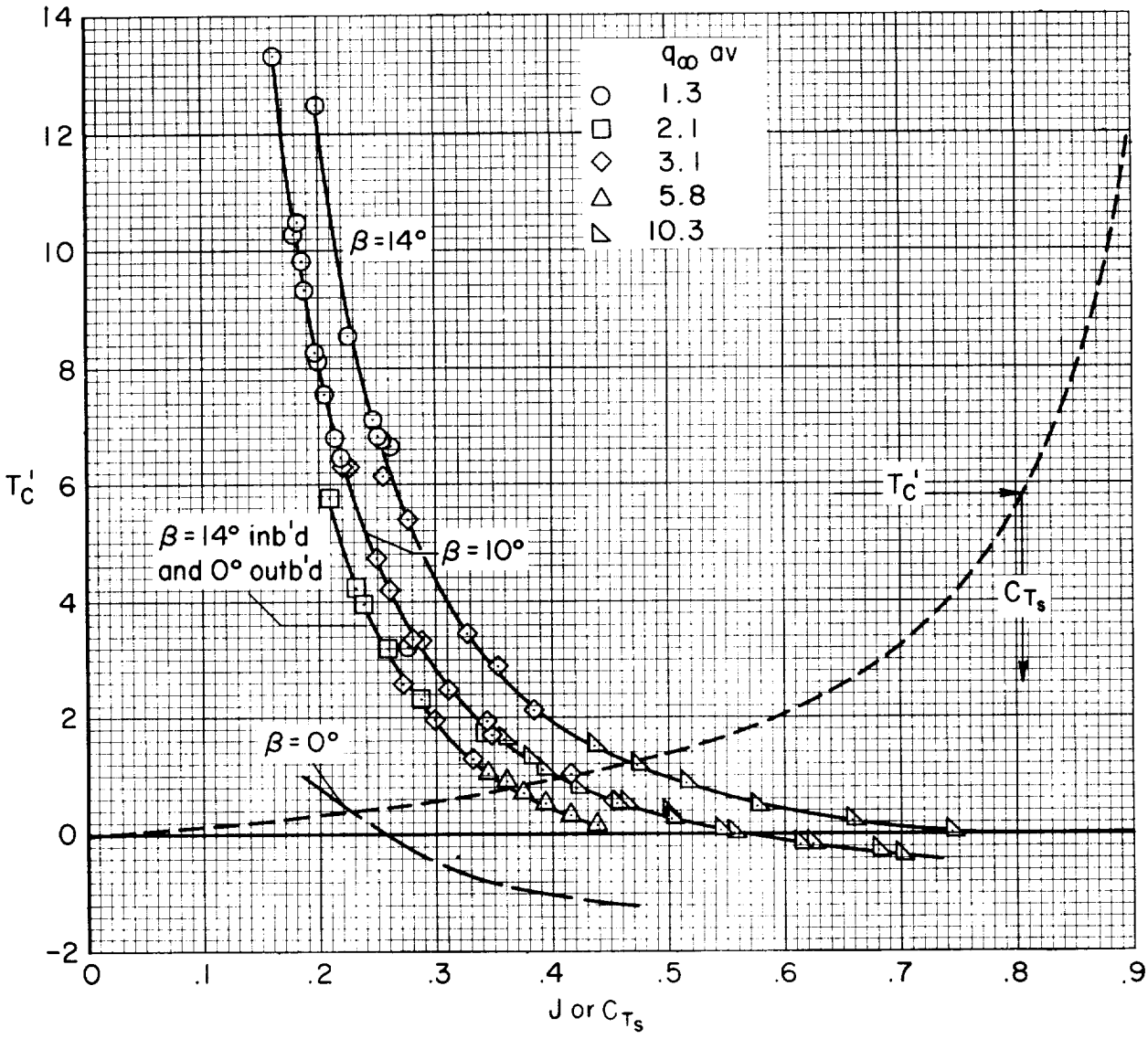

Figure 8.- Propeller thrust characteristics.

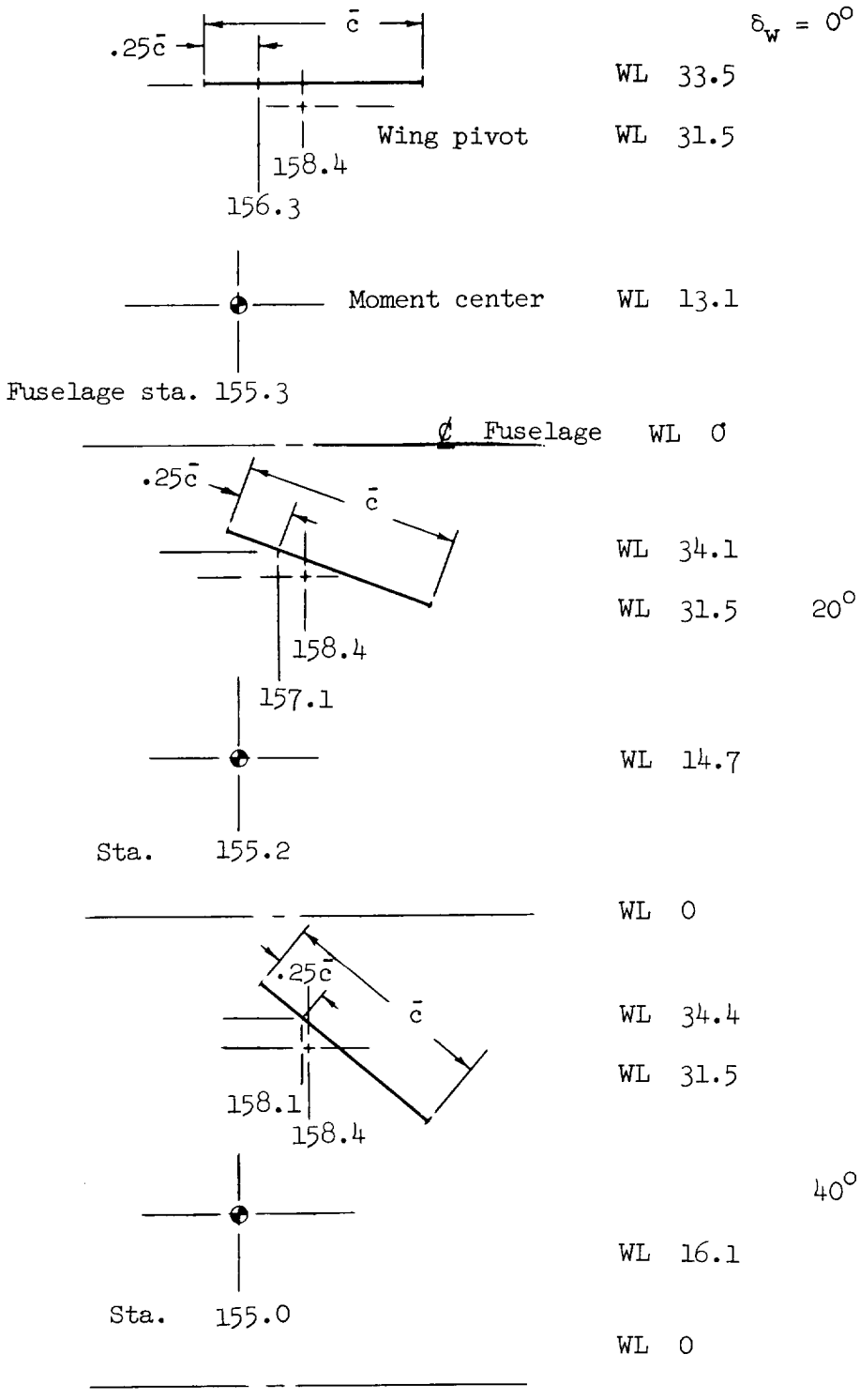

Figure 9.- Variation of pitching-moment center with wing tilt angle.

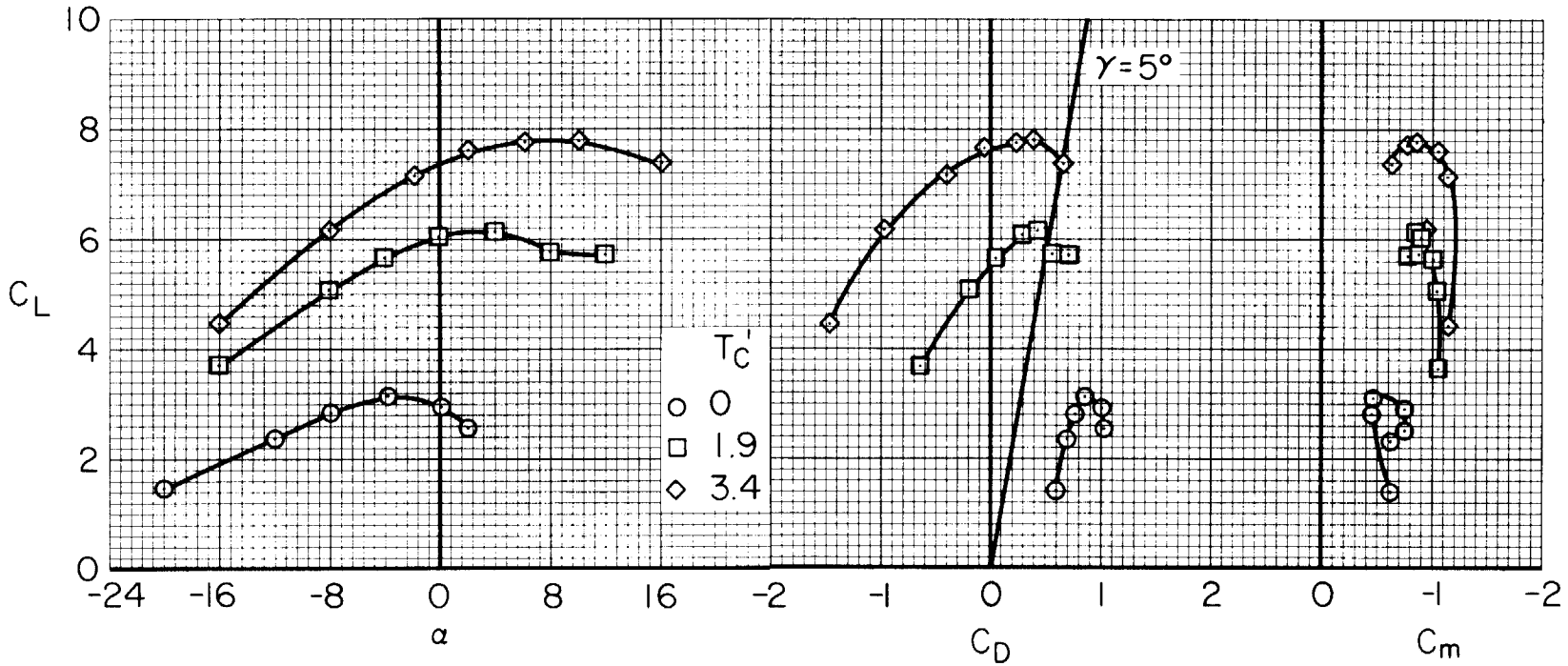

Figure 10.- Longitudinal characteristics of basic model configuration with a wing tilt of 20; $\delta_f = 60°$, partial-span Krüger flaps, $i_t = 20°$.

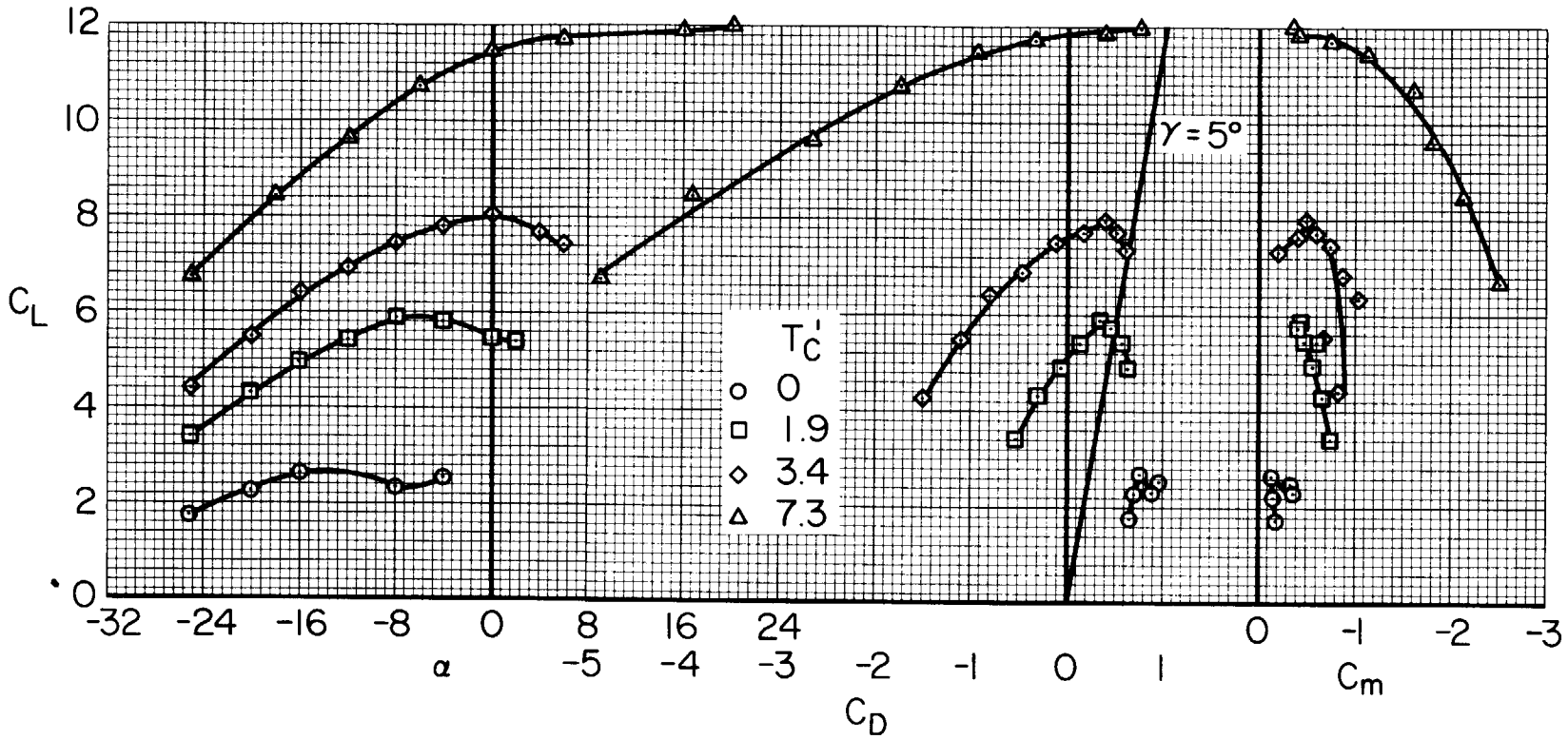

Figure 11.- Longitudinal characteristics of basic model configuration with a wing tilt of 30° and $\delta_f = 60^{\circ}$.

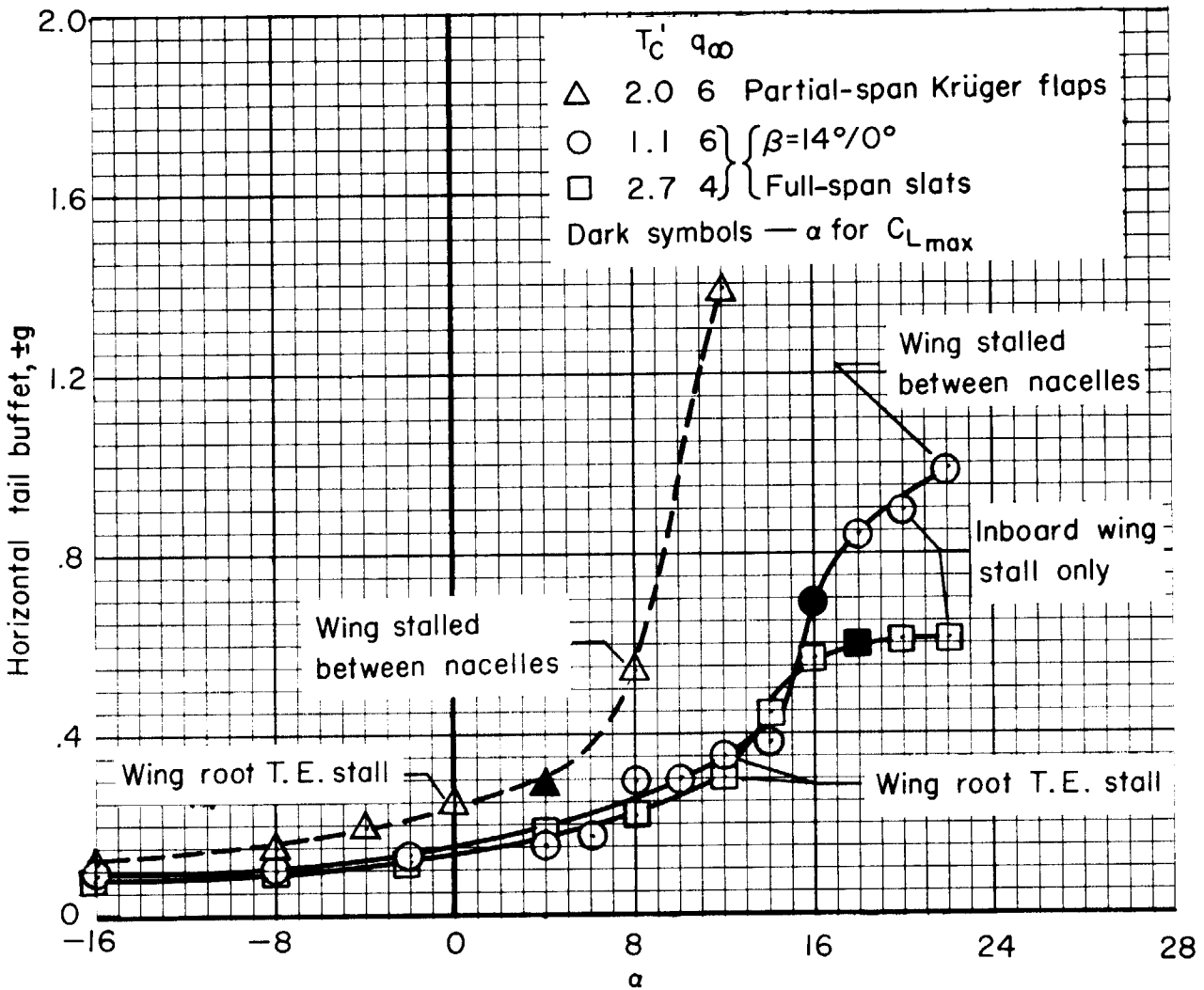

Figure 12.- Buffet intensity of the horizontal tail for two configurations with a wing tilt of 20° $\delta_f = 60°$.

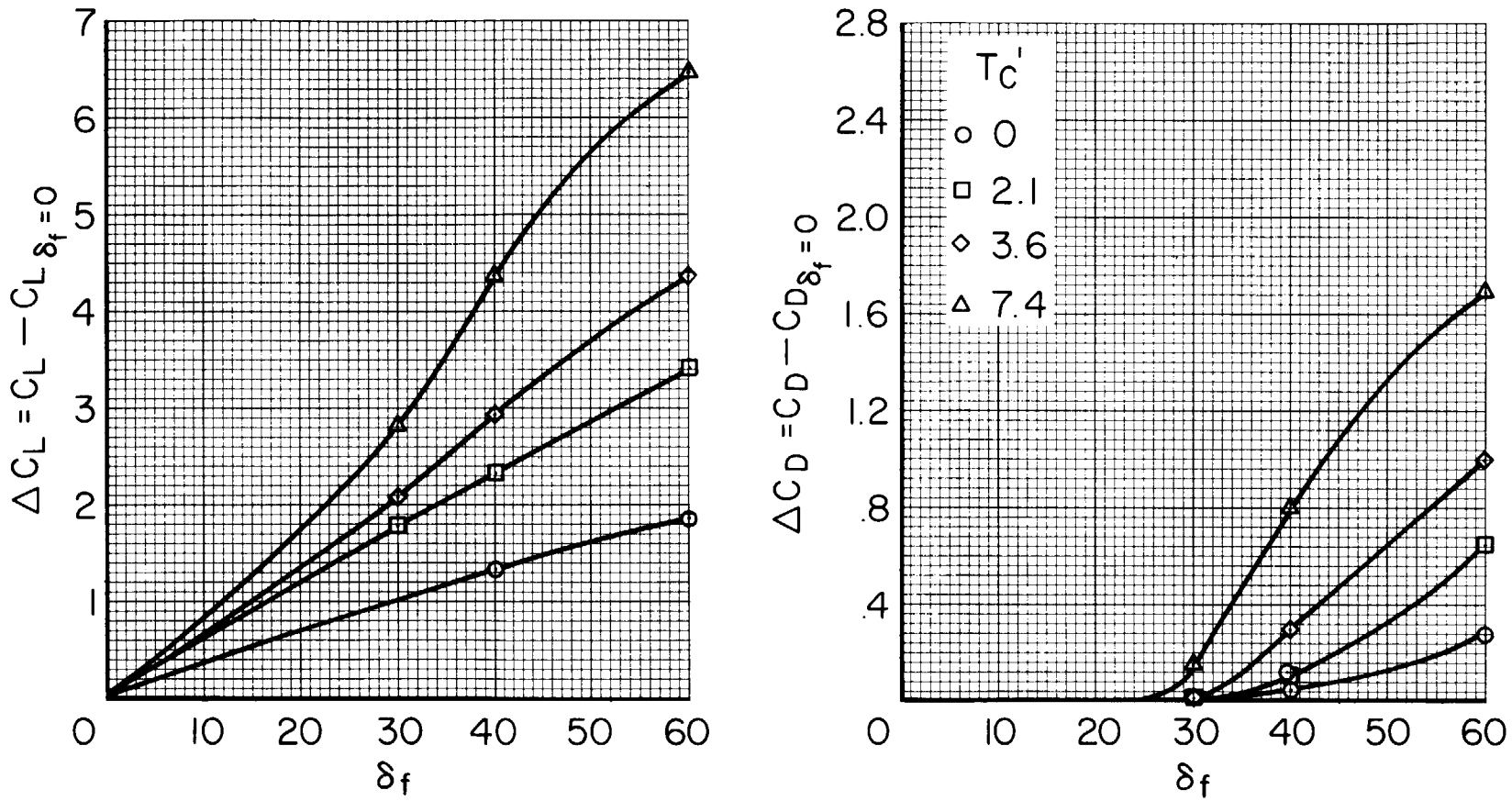

Figure 13.- Effectiveness of trailing-edge flap with wing at 0°; $\alpha = 0^\circ$, $\beta = 10^\circ$, clean leading edge.

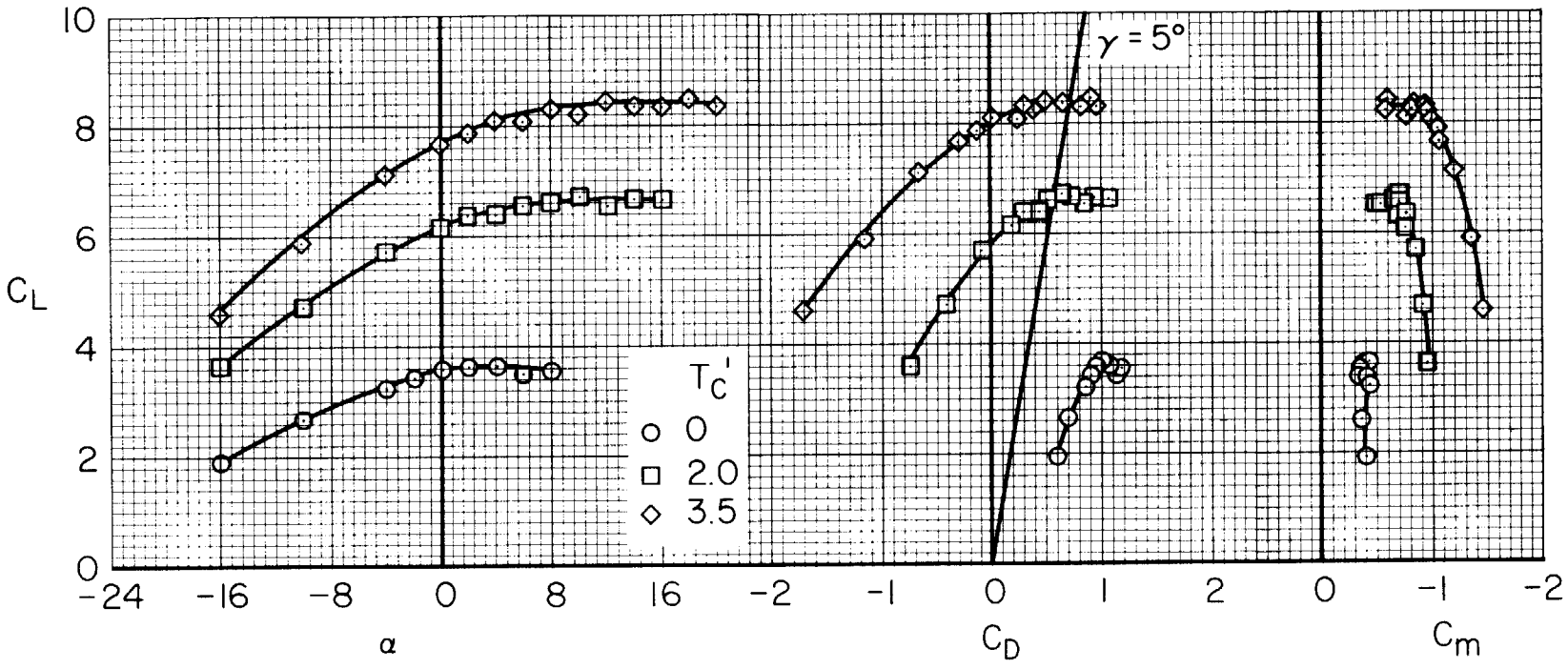

Figure 14.- Longitudinal characteristics of the model with a wing tilt of 20°; $\delta_f = 60^\circ$, full-span slats, $i_t = 20^\circ$, $\beta = 10^\circ$.

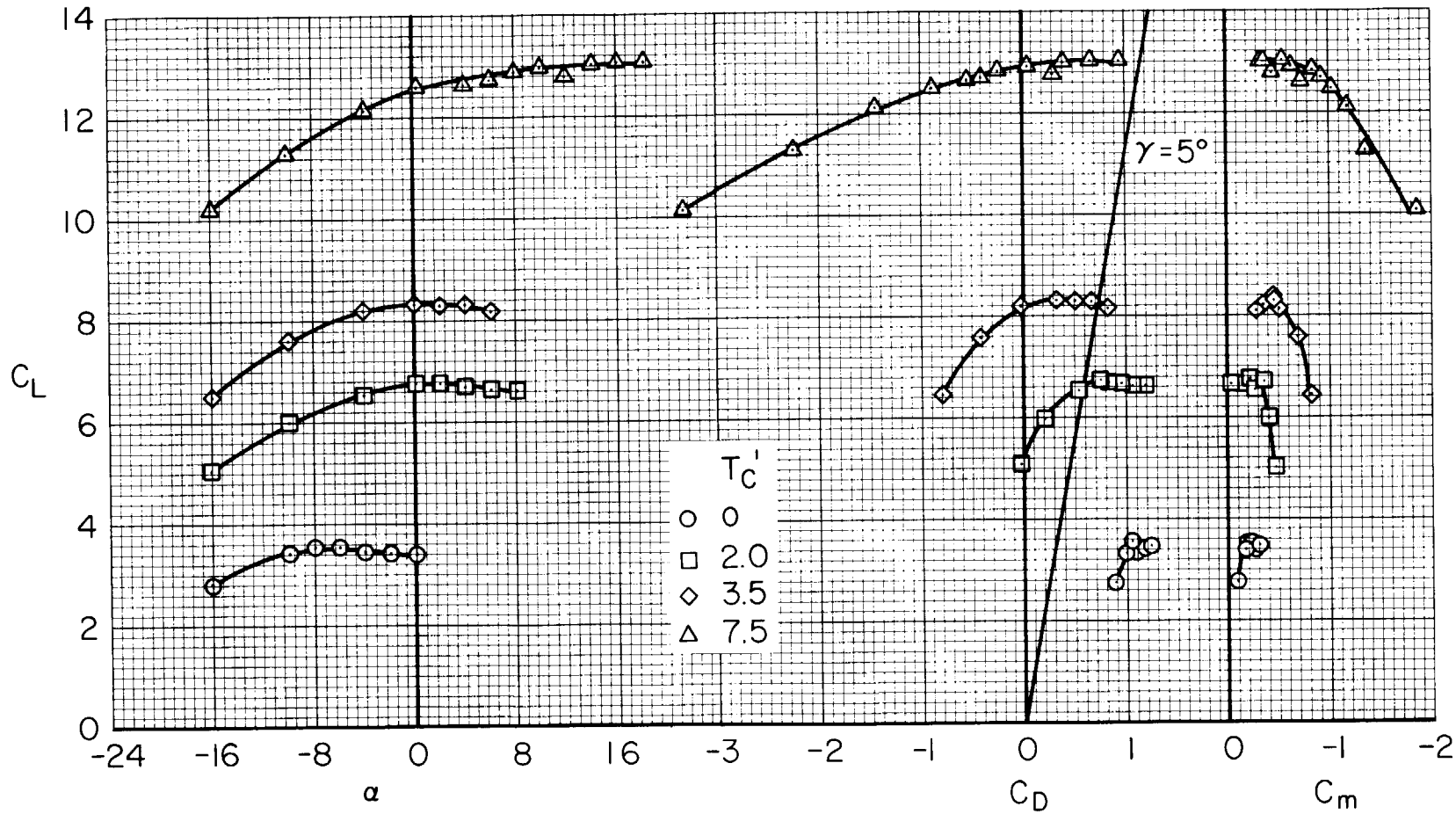

Figure 15.- Longitudinal characteristics of the model with a wing tilt of 30°; δ_f = 60°, full-span slats, i_t = 20°, β = 10°.

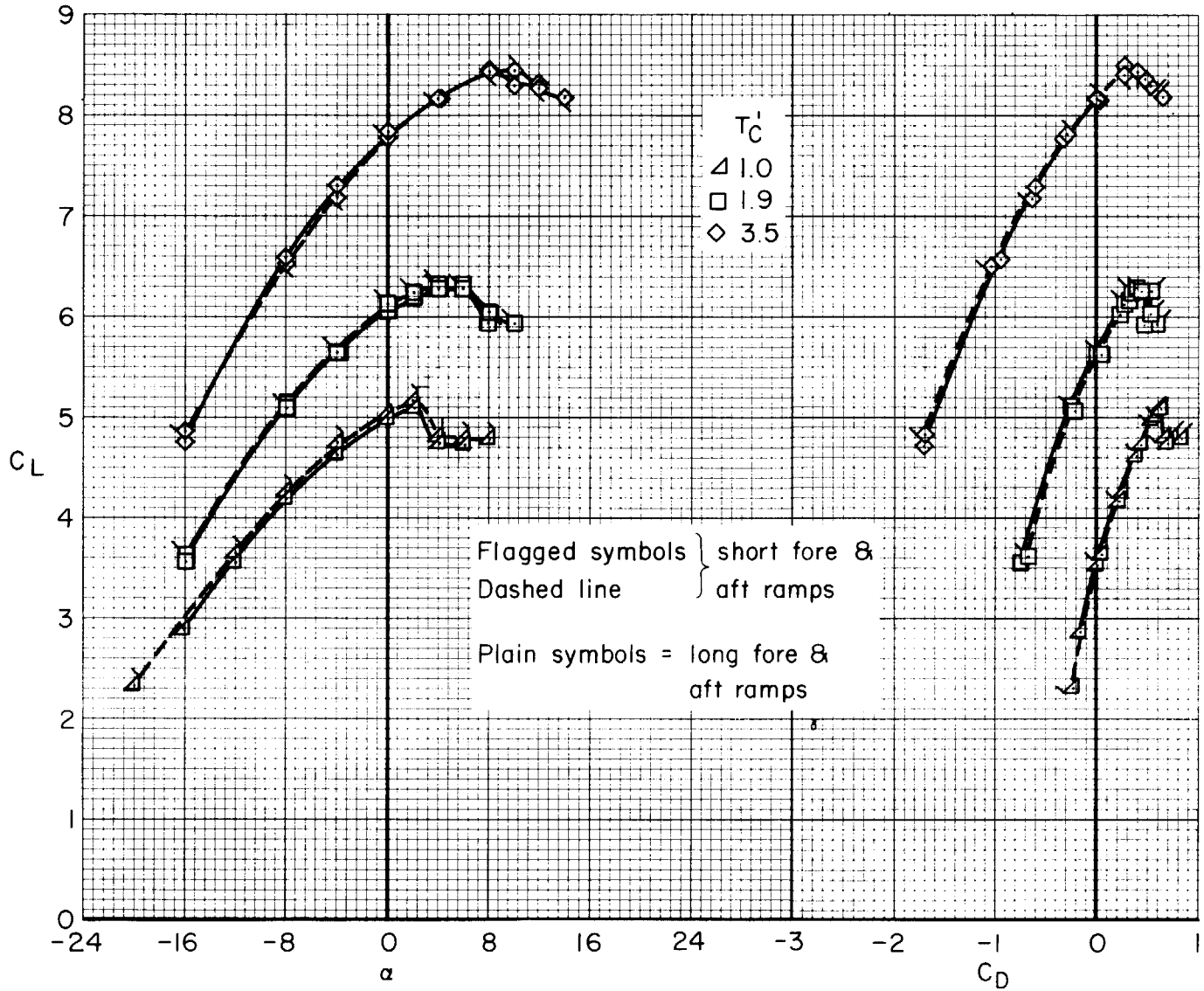

Figure 16.- Force characteristics for two different ramp configurations with a wing tilt of 20°; $\delta_f = 60°$, $\beta = 10°$.

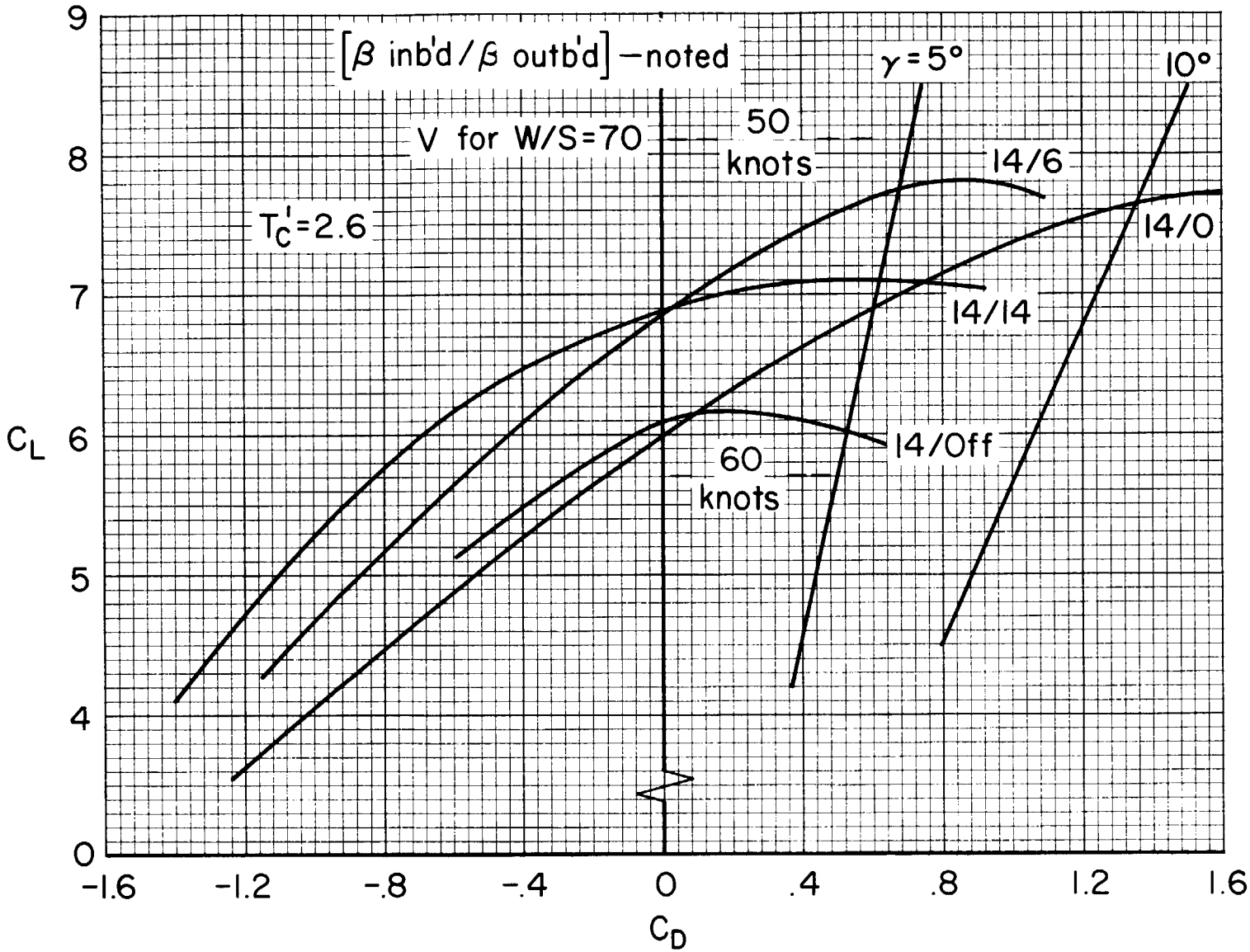

Figure 17.- Effect of differential blade angles with a wing tilt of 20°; δ_f = 60°, full-span slats, i_t = 20°.

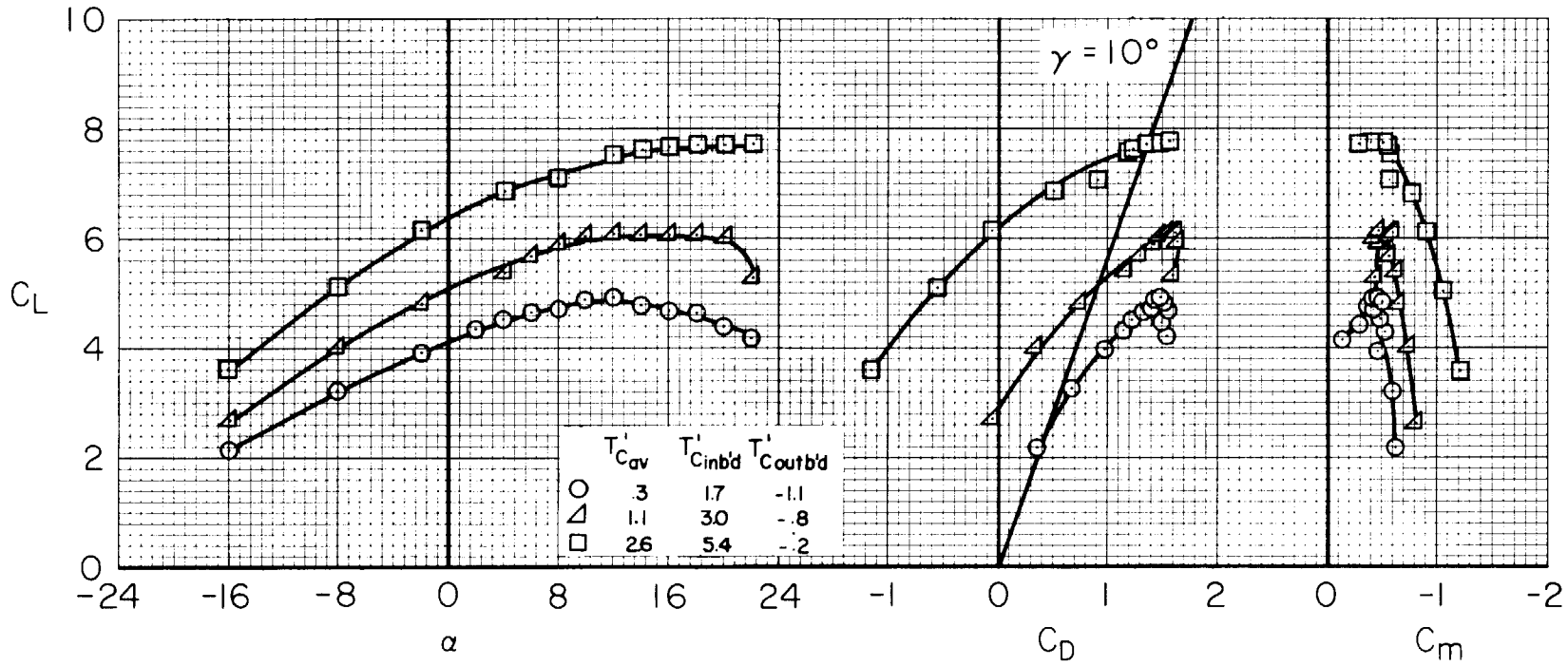

Figure 18.- Longitudinal characteristics of the model with a wing tilt of 20°; δ_f = 60°, full-span slats, β = 14/0, i_t = 20°.

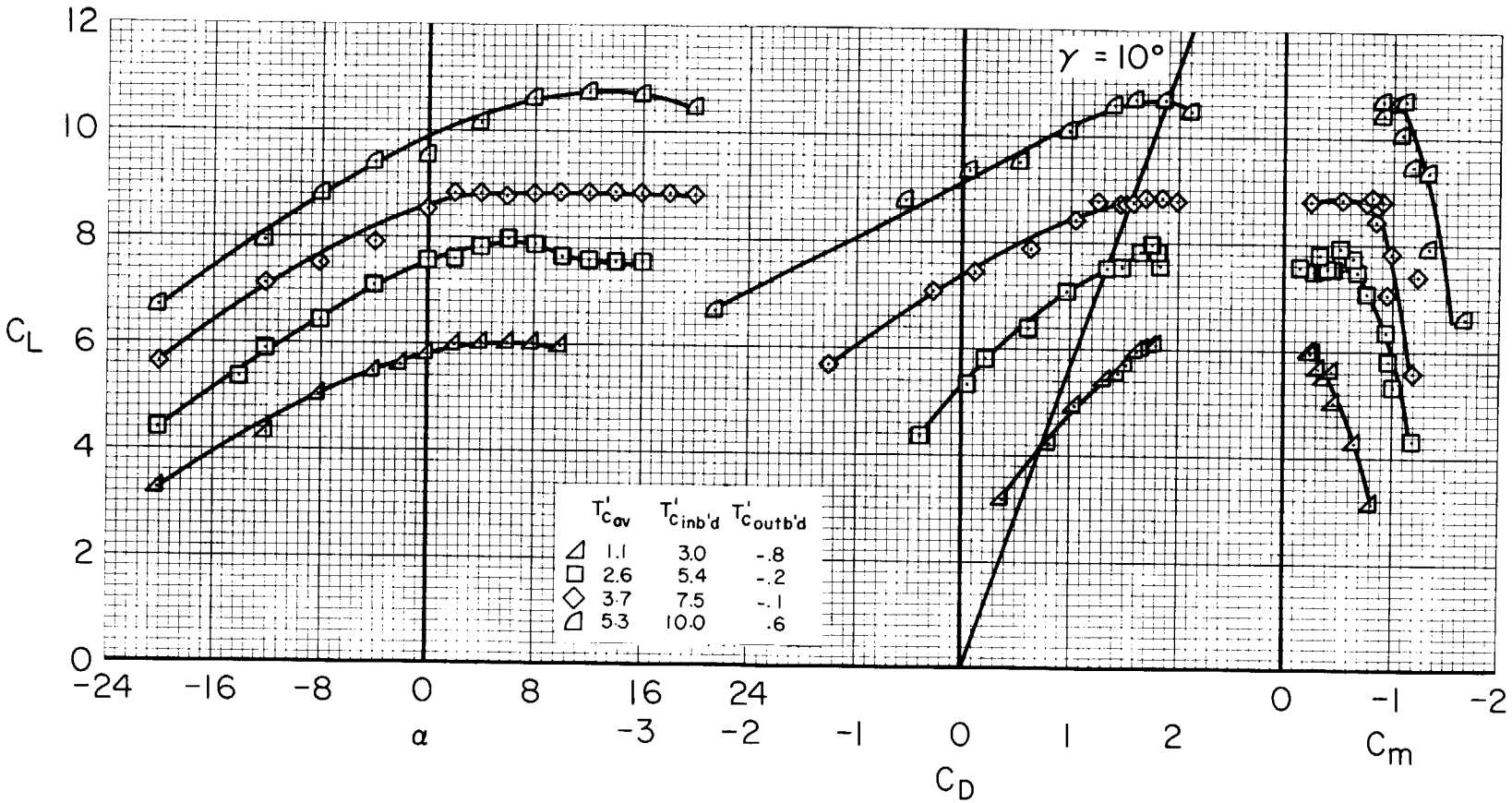

Figure 19.- Longitudinal characteristics of the model with a wing tilt of 30°; δ_f = 60°, full-span slats, β = 14/0, i_t = 20°.

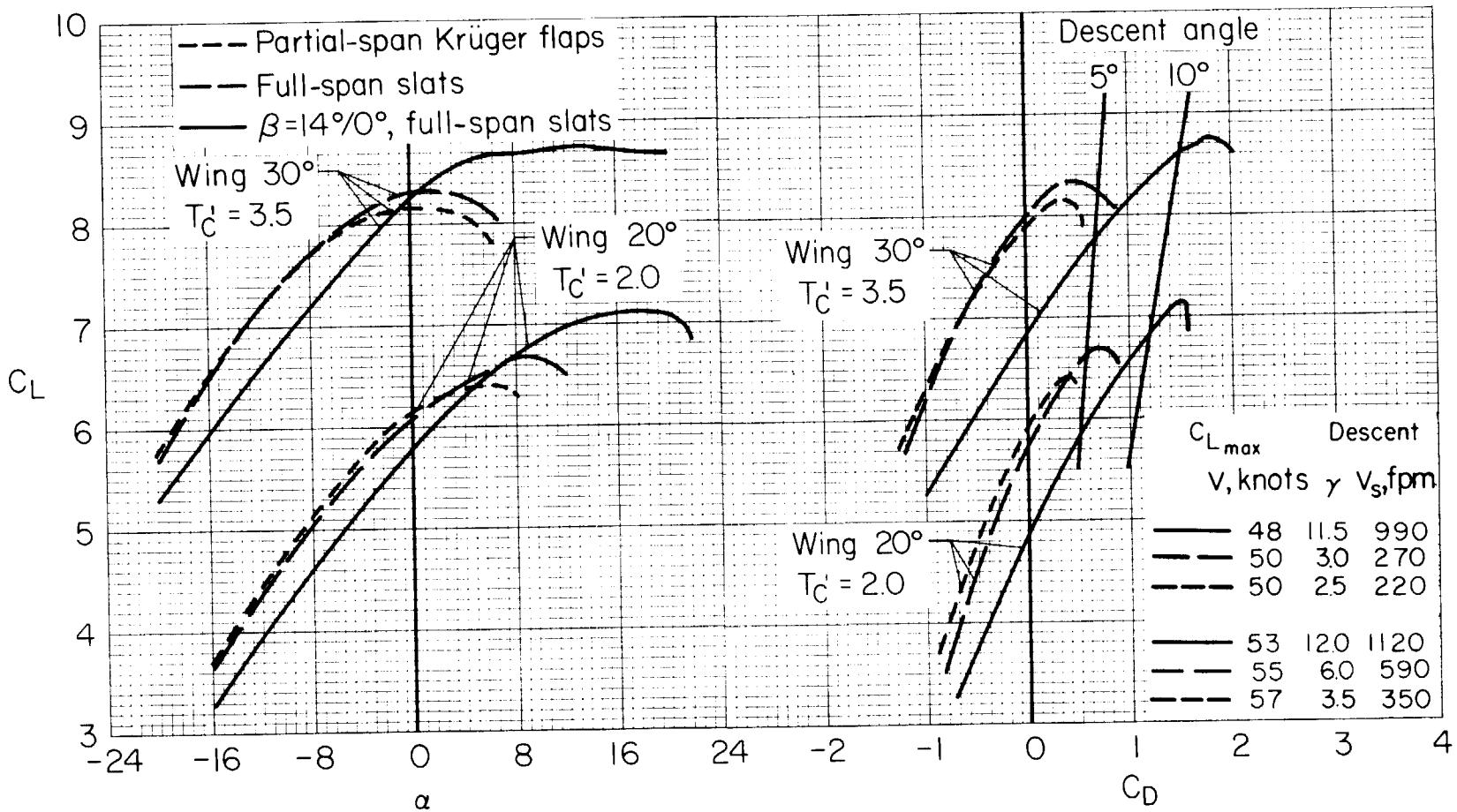

Figure 20.- Summary of force data for three configurations in the transitional regime.

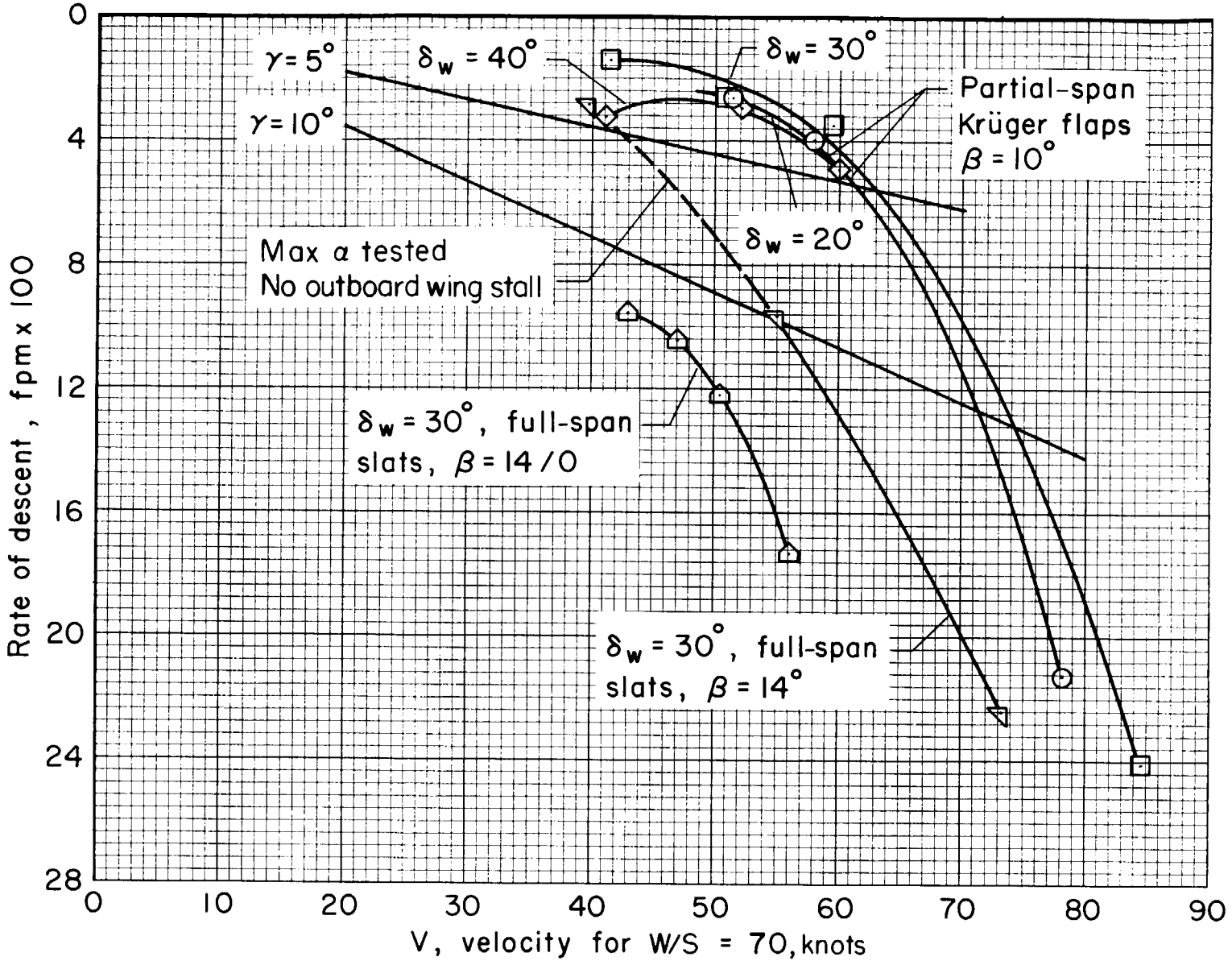

Figure 21.- Summary of descent performance for several configurations.

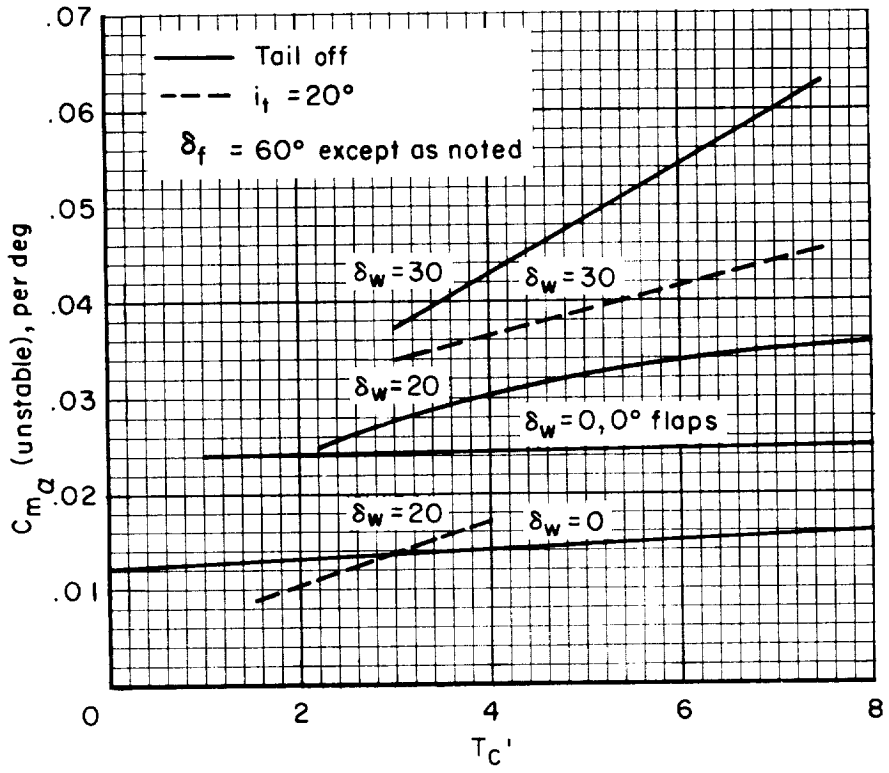

Figure 22.- Longitudinal static stability with partial-span Krüger flaps at various wing tilt angles; α = 0°.

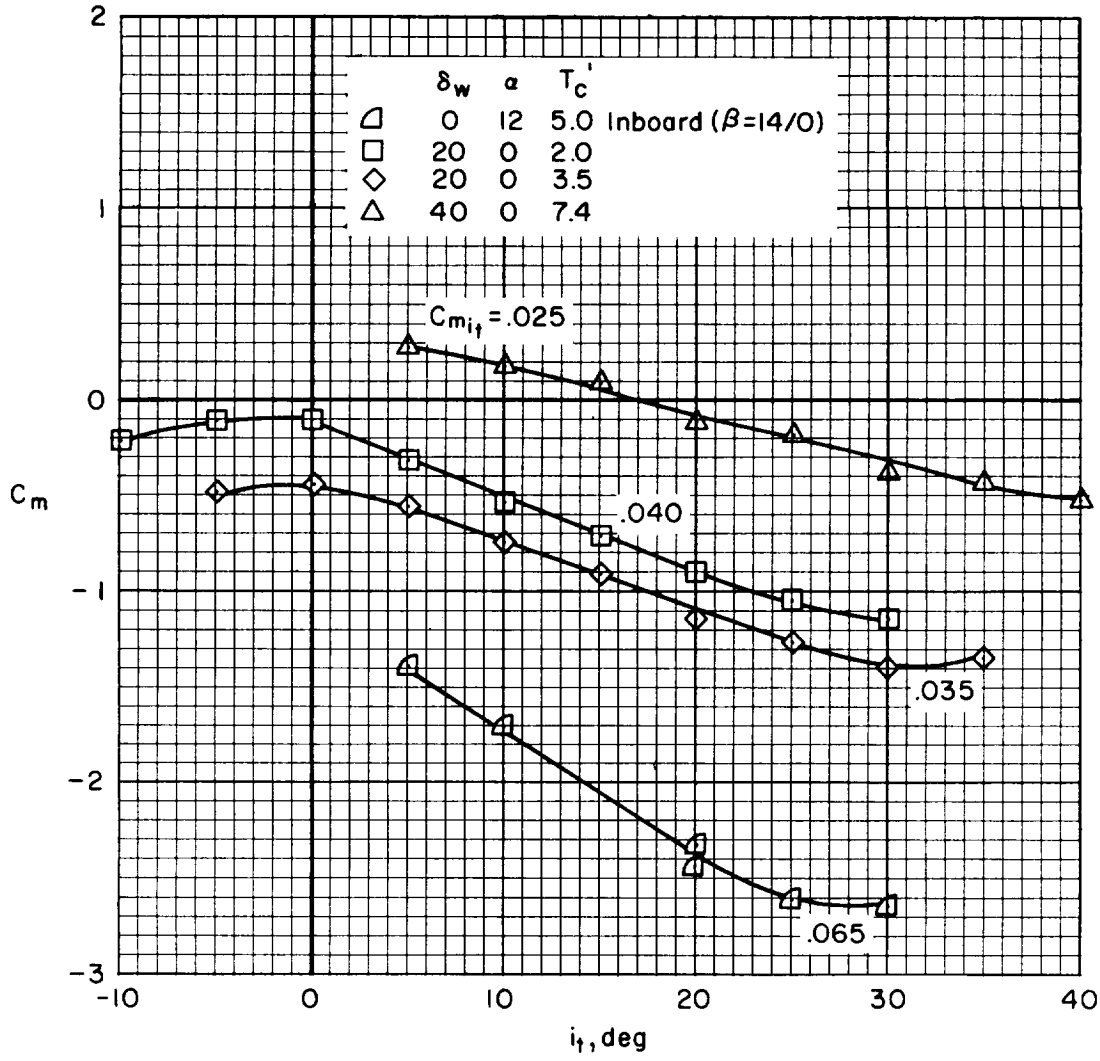

Figure 23.- Effectiveness of horizontal tail with short, fore and aft center-section ramps at various wing tilt angles; $\delta_f = 60^\circ$.

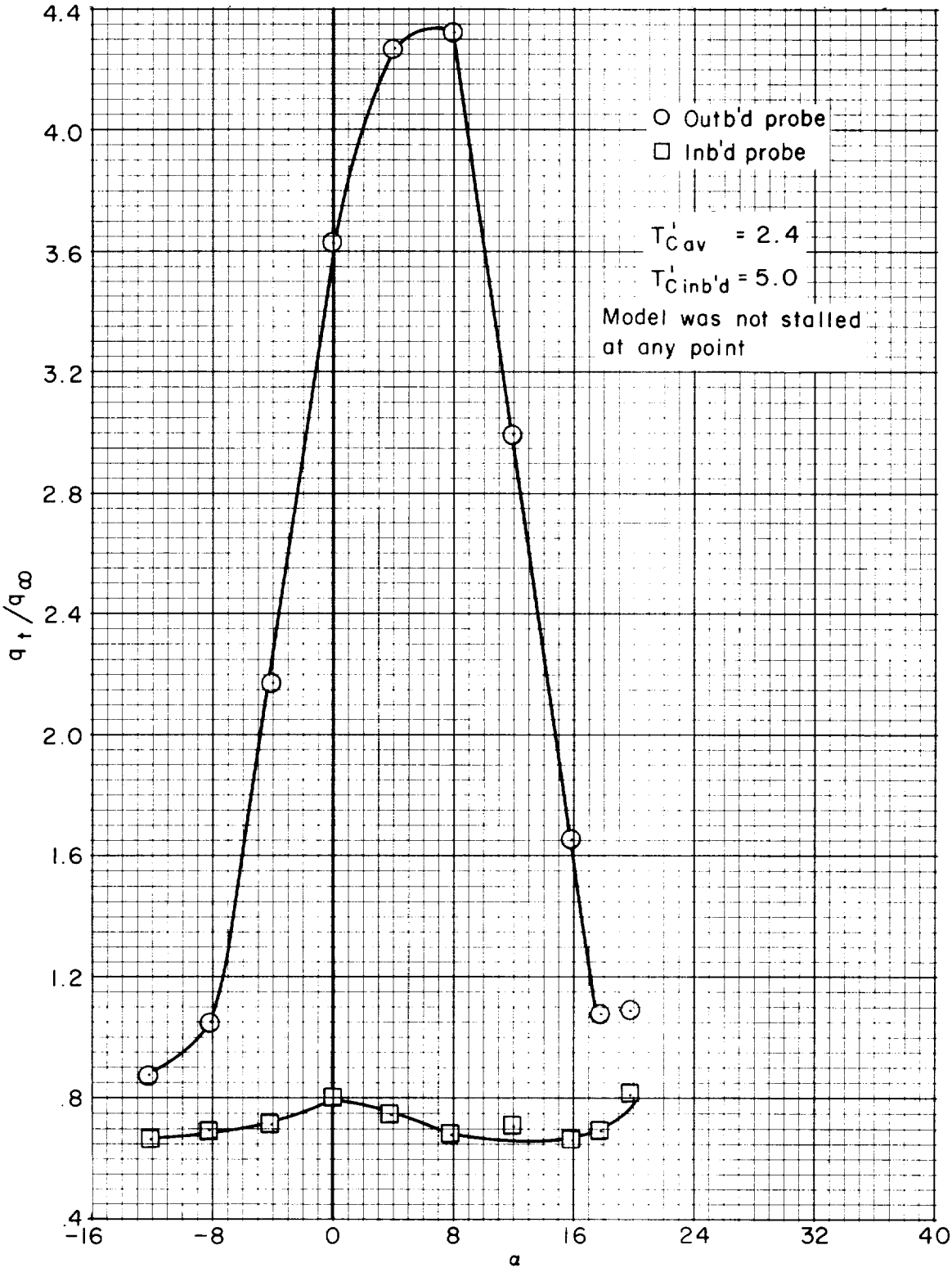

Figure 24.- Dynamic-pressure variation at the horizontal tail; wing tilt of 0°, $\delta_f = 60^\circ$, clean leading edge, $\beta = 14/0$, $i_t = 20^\circ$.

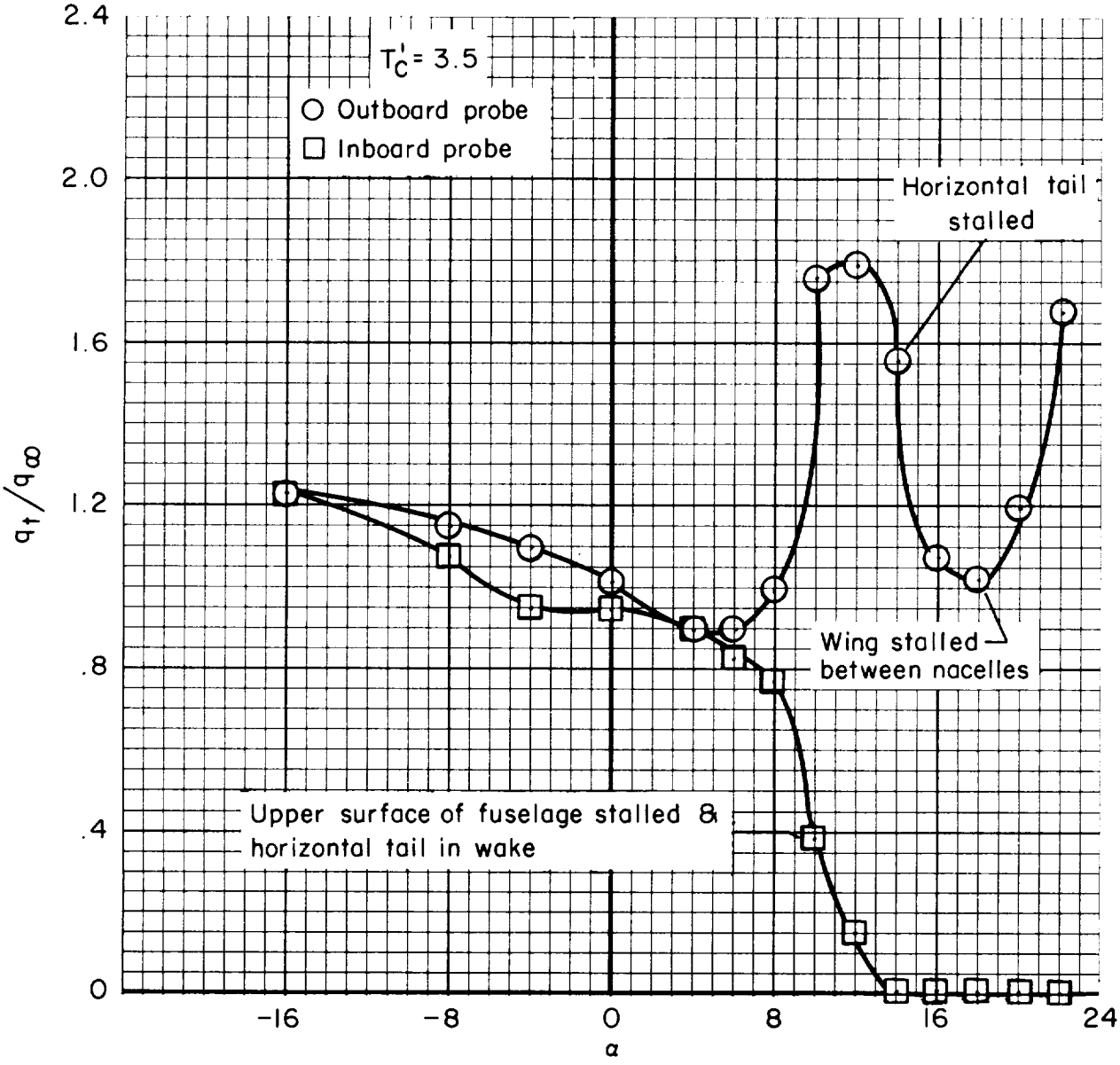

Figure 25.- Dynamic-pressure variation at the horizontal tail; wing tilt of 20°, δ_f = 60°, leading-edge slat outboard of inboard nacelle, β = 10°, i_t = 20°.

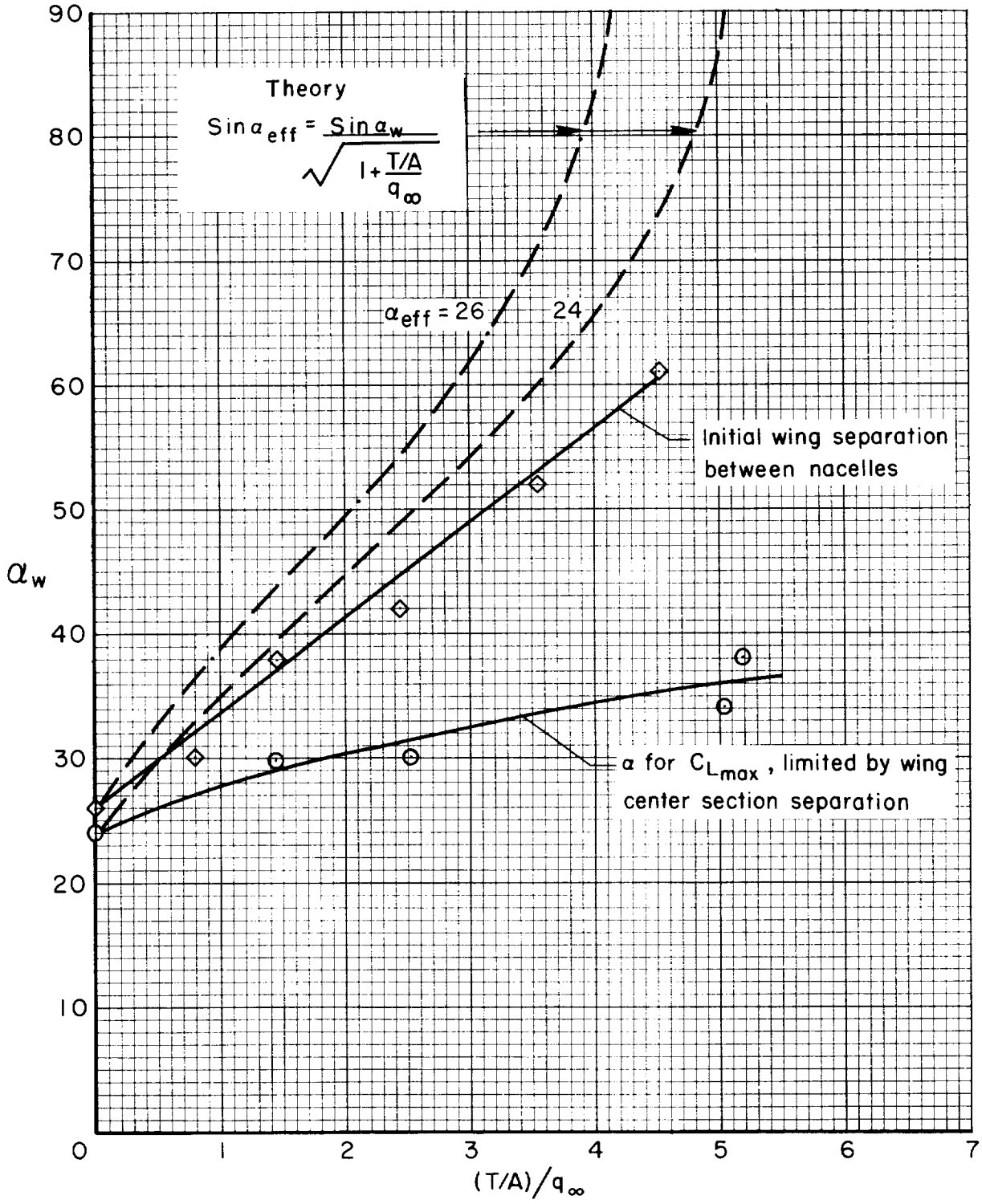

Figure 26.- Comparison of theoretical and experimental angle of attack for wing stall; leading-edge full-span slats, trailing-edge flaps deflected 60°.

"The aeronautical and space activities of the United States shall be conducted so as to contribute . . . to the expansion of human knowledge of phenomena in the atmosphere and space. The Administration shall provide for the widest practicable and appropriate dissemination of information concerning its activities and the results thereof."

—NATIONAL AERONAUTICS AND SPACE ACT OF 1958

NASA SCIENTIFIC AND TECHNICAL PUBLICATIONS

TECHNICAL REPORTS: Scientific and technical information considered important, complete, and a lasting contribution to existing knowledge.

TECHNICAL NOTES: Information less broad in scope but nevertheless of importance as a contribution to existing knowledge.

TECHNICAL MEMORANDUMS: Information receiving limited distribution because of preliminary data, security classification, or other reasons.

CONTRACTOR REPORTS: Technical information generated in connection with a NASA contract or grant and released under NASA auspices.

TECHNICAL TRANSLATIONS: Information published in a foreign language considered to merit NASA distribution in English.

TECHNICAL REPRINTS: Information derived from NASA activities and initially published in the form of journal articles.

SPECIAL PUBLICATIONS: Information derived from or of value to NASA activities but not necessarily reporting the results of individual NASA-programmed scientific efforts. Publications include conference proceedings, monographs, data compilations, handbooks, sourcebooks, and special bibliographies.

Details on the availability of these publications may be obtained from:

SCIENTIFIC AND TECHNICAL INFORMATION DIVISION

NATIONAL AERONAUTICS AND SPACE ADMINISTRATION

Washington, D.C. 20546